Electronic Supplementary Information for

Conjugated polymers of an oxa[5]helicene-derived polycyclic heteroaromatic: tailoring energy levels and compatibility for high-performance perovskite solar cells

Yaohang Cai[a,‡], Yuyan Zhang[a,‡], Lingyi Fang[a], Yutong Ren[a], Jidong Zhang[b], Yi Yuan[a], Jing Zhang[a], and Peng Wang[a,*]

[a]*State Key Laboratory of Silicon and Advanced Semiconductor Materials, Department of Chemistry, Zhejiang University, Hangzhou 310058, China.*
[b]*State Key Laboratory of Polymer Physics and Chemistry, Changchun Institute of Applied Chemistry, Chinese Academy of Sciences, Changchun, 130022, China*

---

* Corresponding author.
E-mail addresses: pw2015@zju.edu.cn.

‡ These authors contributed equally to this work.

1 Experimental section

1.1 Reagents and materials

Bis(pinacolato)diboron (98%, Energy Chemical), [1,1'-bis(diphenylphosphino)ferrocene]dichloropalladium(II) ($Pd(dppf)Cl_2$, 98%, Pd > 14.5%, Energy Chemical), potassium acetate (KOAc, 99%, Energy Chemical), palladium diacetate ($Pd(OAc)_2$, 99%, Energy Chemical), 2-dicyclohexylphosphino-2',6'-dimethoxybiphenyl (SPhos, 98%, Energy Chemical), potassium phosphate (K_3PO_4, 99%, Energy Chemical), Amberlyst® 15 hydrogen form (dry, Energy Chemical), *N*-bromosuccinimide (NBS, 98%, Energy Chemical), tris(dibenzylideneacetone)dipalladium ($Pd_2(dba)_3$, 98%, Energy Chemical), tris(2-methoxyphenyl)phosphine ((*o*MeOPh)$_3$P, 97%, Energy Chemical), *N,N,N',N'*-tetramethylethylenediamine (TMEDA, 99%, Energy Chemical), pivalic acid (PivOH, 99%, Energy Chemical), cesium carbonate (Cs_2CO_3, 99.9%, Energy Chemical), disodium dihydrogen ethylenediaminetetraacetate dihydrate (EDTA, 99%, Energy Chemical), ferric chloride ($FeCl_3$, anhydrous, 98%, Energy Chemical), 1-ethyl-3-methylimidazolium bis(trifluoromethanesulfonyl)imide (EMITFSI, 98%, Energy Chemical), ferrocene (97%, Aldrich), PEDOT:PSS (AI 4083, Heraeus® Clevios), benzocyclobutene (BCB, 98%, Energy Chemical), 4-*tert*-butylpyridine (TBP, 96%, Sigma-Aldrich), polystyrene (PS, typical M_w ~ 280,000, Sigma-Aldrich), tin(IV) oxide (SnO_2, 15% hydrocolloid dispersion, Alfa Aesar), lead(II) iodide(PbI_2, 99.99%, TCI), rubidium chloride (RbCl, 99.9%, 3A), formamidinium iodide (FAI, 99.0%, Greatcell Solar), methylamine hydrochloride (MACl, 98%, TCI), triphenylmethane-4,4',4''-triisocyanate (TTI, 20% solution in chlorobenzene, Aladdin), and N^2,N^2,$N^{2'}$,$N^{2'}$,N^7,N^7,$N^{7'}$,$N^{7'}$-octakis(4-methoxyphenyl)-9,9'-spirobi[fluorene]-2,2',7,7'-tetraamine (spiro-OMeTAD, 99.8%, Xi'an Polymer Light Technology Corp.) were procured from commercial sources and employed without further purification. Solvents including 1,4-dioxane (99%, Energy Chemical), tetrahydrofuran (THF), toluene, deuterated tetrahydrofuran (THF-d_8, 99%, J&K Scientific), tetrahydrofuran (THF, Water ≤ 50 ppm, 99.5%, Energy Chemical), acetone (≥ 99.5%, Sinopharm Chemical Reagent Co., Ltd), ethanol (99.7%, Aladdin), chlorobenzene (CB, 99.8%, Acros Organics), dimethyl sulfoxide (DMSO, 99.9%, Sigma-Aldrich), *N*,*N*-dimethylformamide (DMF, Water ≤ 30 ppm, 99.9%, Energy Chemical), 2-propanol (IPA, 99.5%, Sigma-Aldrich), and acetonitrile (MeCN, ≥ 99.9%, Energy Chemical) were also purchased from commercial suppliers and employed without further purification. 5,9-Dibromodinaphtho[2,1-*b*:1',2'-*d*]furan (**1**),[1] *n*-butyl 2-bromothiophene-3-carboxylate,[2] (4-hexylphenyl)magnesium bromide,[2] 5,5'-(2,5-bis(hexyloxy)-1,4-phenylene)bis(3,4-ethylenedioxythiophene) (EBEH),[3] and 4-*tert*-butylpyridinium bis(trifluoromethanesulfonyl)imide (TBPHTFSI)[4] were synthesized according to the corresponding literature procedures.

1.2 General instrumentation

Melting point determinations were conducted using the WRS-1B digital melting point apparatus (INESA). Nuclear magnetic resonance (NMR) spectroscopy, covering ^{1}H and ^{13}C NMR, was performed on an AVANCE III 500 spectrometer from Bruker. All chemical shifts were referenced to THF-d_8. High-resolution mass spectrometry (HR-MS) measurements were recorded on a 6545 LC/Q-TOF system (Agilent). Attenuated total reflection-Fourier transform infrared (ATR-FTIR) spectroscopy measurements were carried out utilizing a Thermo Scientific™ Nicolet™ iS50 FTIR spectrometer. Ultraviolet-visible (UV-vis) absorption spectra were acquired with a Cary 8454 spectrophotometer (Agilent Technologies). Carbon and hydrogen content analyses were conducted employing the Vario Micro cube element analyzer (Elementar Analysensysteme GmbH). High temperature gel permeation chromatography (HT-GPC) measurements were performed using a PL-GPC220 instrument (Polymer Laboratories Ltd.), with 1,2,4-trichlorobenzene as the eluent. Differential scanning calorimetry (DSC) measurements were executed on a DSC Q100 V9.7 Build 291 instrument (TA) under a flowing nitrogen atmosphere, employing a heating rate of 10°C min^{-1}.

1.3 Synthesis

The synthesis of DTPF4 monomer and DTPF4-2Br monomer adhered to the prescribed routes outlined in Scheme S1. Furthermore, the synthetic pathways of DTPF4-based conjugated polymers and p-EBEH are elaborated in Scheme S2. Comprehensive synthetic procedures are also provided as follows.

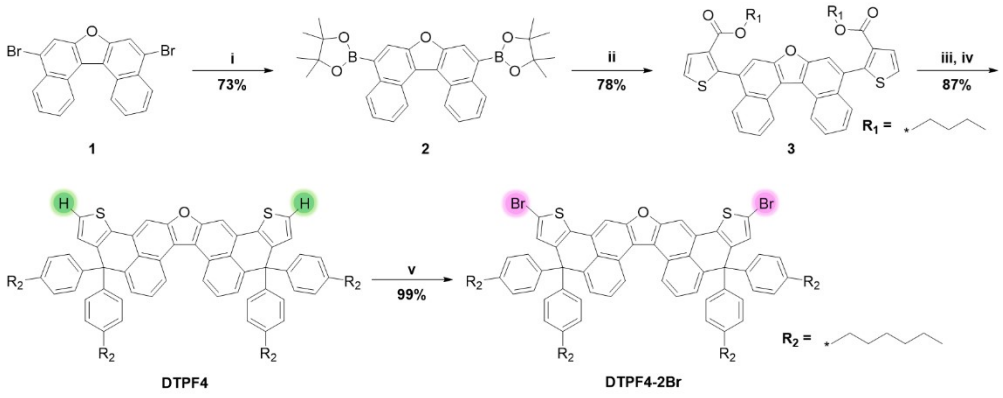

Scheme S1. Synthetic routes for monomers DTPF4 and DTPF4-2Br. Reagents and conditions: (i) bis(pinacol)diborane, $Pd(dppf)Cl_2$, KOAc, 1,4-dioxane, reflux, overnight; (ii) *n*-butyl 2-bromothiophene-3-carboxylate, $Pd(OAc)_2$, SPhos, K_3PO_4, 1,4-dioxane/H_2O (*v*/*v*, 5/1), reflux, overnight; (iii) (4-hexylphenyl)magnesium bromide, THF, reflux, overnight; (iv) Amberlyst 15, toluene, reflux, 5 hours; (v) *N*-bromosuccinimide, THF, room temperature, 1 hour. R_1 and R_2 refer to *n*-butyl and *n*-hexyl, respectively.

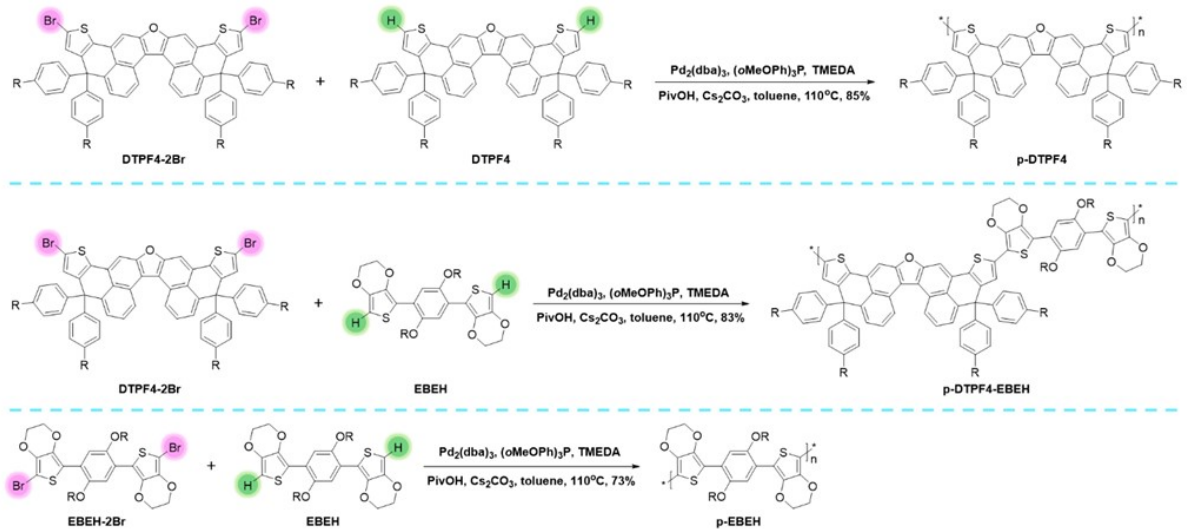

Scheme S2. Conjugated polymers prepared via Pd-catalyzed direct arylation polycondensation. R represents *n*-hexyl.

1.3.1 5,9-Bis(4,4,5,5-tetramethyl-1,3,2-dioxaborolan-2-yl)dinaphtho[2,1-*b*:1',2'-*d*]furan (2)

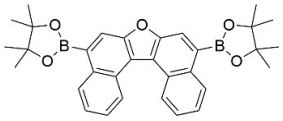

In a 500 mL round bottom flask, 5,9-dibromodinaphtho[2,1-*b*:1',2'-*d*]furan (**1**) (4.26 g, 10.00 mmol), bis(pinacol)diborane (6.35 g, 25.00 mmol), Pd(dppf)Cl_2 (0.29 g, 0.40 mmol), KOAc (3.93 g, 40.00 mmol) and 1,4-dioxane (250 mL) were combined. The reaction mixture underwent overnight reflux under an argon atmosphere. Upon cooling to room temperature, the organic solvent was removed under vacuum, followed by the addition of water (100 mL). After three successive extractions with dichloromethane (3 × 100 mL), the combined organic phases were washed with water and dried over anhydrous sodium sulfate. Subsequent solvent evaporation afforded the crude material, which was purified by column chromatography (eluent: toluene), yielding the desired compound as a white solid (3.80 g, 73% yield). Melting point: 255–256°C. ^{1}H NMR (500 MHz, THF-d_8) δ: 9.17 (d, J = 8.4 Hz, 2H), 9.10 (d, J = 8.3 Hz, 2H), 8.44 (s, 2H), 7.72 (t, J = 7.5 Hz, 2H), 7.59 (t, J = 7.5 Hz, 2H), and 1.47 (s, 24H) ppm. ^{13}C NMR (125 MHz, THF-d_8) δ: 155.23, 135.88, 131.02, 129.89, 126.69, 126.56, 125.71, 122.88, 122.84, 85.06, and 25.42 ppm. HR-MS (ESI) m/z calcd. for $([C_{32}H_{34}B_2O_5]^+Na)^+$: 543.2485. Found: 543.2488. ATR-FTIR (film) ν_{max} = 2976, 1578, 1389, 1305, 1255, 1231, 1140, 1130, 981, 897, 851, 757, and 676 cm^{-1}. UV-vis (THF) λ_{max}: 360 and 377 nm. Elemental analysis calcd. for $C_{32}H_{34}B_2O_5$: C 73.88 and H 6.59. Found: C 73.87 and H 6.61.

1.3.2 Dibutyl 2,2'-(dinaphtho[2,1-*b*:1',2'-*d*]furan-5,9-diyl)bis(thiophene-3-carboxylate) (3)

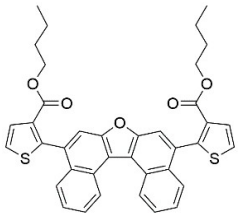

In a 250 mL round-bottom flask, compound **2** (3.12 g, 6.00 mmol), *n*-butyl 2-bromothiophene-3-carboxylate (3.95 g, 15.00 mmol), $Pd(OAc)_2$ (67.4 mg, 0.30 mmol), SPhos (0.12 g, 0.30 mmol), K_3PO_4 (6.37 g, 30.00 mmol), water (20 mL), and 1,4-dioxane (100 mL) were combined. The reaction mixture underwent overnight reflux under an argon atmosphere. Upon cooling to room temperature, the solvents were evaporated under vacuum, followed by the addition of water (100 mL). The resulting mixture underwent three times extractions with dichloromethane (3 × 100 mL). The organic phases were combined, washed with water, and dried over anhydrous sodium sulfate. After solvent removal, the crude product was purified by column chromatography (eluent: toluene) on silica gel, yielding the desired compound as a white solid (2.96 g, 78% yield). Melting point: 168–170°C. ^{1}H NMR (500 MHz, THF-d_8) δ: 9.27 (d, J = 8.4 Hz, 2H), 7.97 (s, 2H), 7.85 (d, J = 8.4 Hz, 2H), 7.80–7.76 (m, 2H), 7.68 (d, J = 5.4 Hz, 2H), 7.63 (d, J = 5.4 Hz, 2H), 7.54 (dd, J = 11.2, 3.9 Hz, 2H), 3.79 (t, J = 5.7 Hz, 4H), 0.91 (m, 4H), 0.69–0.60 (m, 4H), and 0.43 (t, J = 7.3 Hz, 6H) ppm. ^{13}C NMR (125 MHz, THF-d_8) δ: 163.11, 154.76, 147.83, 133.78, 133.34, 132.19, 130.48, 129.55, 128.46, 127.30, 126.65, 126.60, 126.02, 120.75, 115.76, 64.74, 31.28, 19.78, and 13.97 ppm. HR-MS (ESI) m/z calcd. for $([C_{38}H_{32}O_5S_2]^+Na)^+$: 655.1583. Found: 655.1584. ATR-FTIR (film) ν_{max} = 1706, 1400, 1276, 1262, 1152, 1015, 870, 753, and 715 cm^{-1}. UV-vis (THF) λ_{max}: 354 and 370 nm. Elemental analysis calcd. for $C_{38}H_{32}O_5S_2$: C 72.13 and H 5.10. Found: C 72.14 and H 5.13.

1.3.3 4,4,11,11-Tetrakis(4-hexylphenyl)-4,11-dihydrothieno[2',3':4,5]phenaleno[2,1-*b*]thieno[2',3':4,5]phenaleno[1,2-*d*]furan (DTPF4)

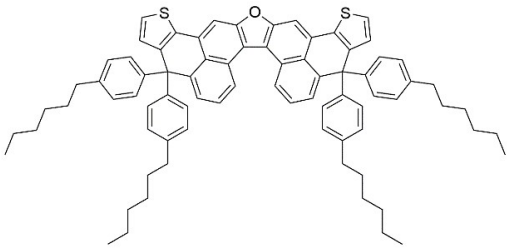

In a flame-dried round-bottom flask, compound **3** (2.53 g, 4.00 mmol), (4-hexylphenyl)magnesium bromide (12 mL, 2 M in THF), and anhydrous THF (80 mL) were meticulously combined. The resulting mixture was subjected to overnight reflux, subsequently cooled to room temperature, and slowly quenched with water. The resulting mixture was introduced into a cold 1 M hydrochloric acid solution, followed by extraction with

dichloromethane (3 × 100 mL). The combined organic extracts thoroughly washed with water and desiccated with anhydrous sodium sulfate. Following solvent evaporation under reduced pressure, the prepared tertiary alcohol was directly utilized in the subsequent reaction. For the subsequent step, the tertiary alcohol was dissolved in toluene (40 mL), to which Amberlyst 15 (0.50 g) was added. The mixture was refluxed for 5 hours. After cooling to room temperature, the mixture was filtered through a Kieselguhr pad, and the filtrate was subjected to vacuum concentration. The crude product underwent purification via column chromatography (eluent: toluene/petroleum ether 60–90°C, *v*/*v*, 1/10) on silica gel, yielding a yellow solid identified as **DTPF4** monomer (3.82 g, 87% yield). Melting point: 183–184°C. ^{1}H NMR (500 MHz, THF-d_8) δ: 8.89 (d, J = 8.3 Hz, 2H), 7.96 (s, 2H), 7.56 (t, J = 7.9 Hz, 2H), 7.41 (d, J = 7.4 Hz, 2H), 7.32 (d, J = 5.2 Hz, 2H), 7.09 (d, J = 8.3 Hz, 8H), 7.04 (d, J = 8.3 Hz, 8H), 6.78 (d, J = 5.2 Hz, 2H), 2.57–2.52 (m, 8H), 1.61–1.53 (m, 8H), 1.37–1.26 (m, 24H), and 0.87 (t, J = 6.5 Hz, 12H) ppm. ^{13}C NMR (125 MHz, THF-d_8) δ: 155.74, 146.87, 146.17, 145.19, 141.83, 135.91, 131.34, 130.67, 129.70, 129.23, 129.01, 128.77, 126.83, 125.80, 125.21, 125.15, 120.10, 106.30, 59.53, 36.47, 32.85, 32.62, 30.26, 23.64, and 14.58 ppm. HR-MS (ESI) *m*/*z* calcd. for ($[C_{78}H_{80}OS_2]^+Na)^+$: 1119.5543. Found: 1119.5542. ATR-FTIR (film) ν_{max} = 2952, 2922, 2852, 1508, 1455, 1321, 1192, 1057, 1021, 844, 763, 726, and 664 cm^{-1}. UV-vis (THF) λ_{max}: 401, 425, and 453 nm. Elemental analysis calcd. for $C_{78}H_{80}OS_2$: C 85.35 and H 7.35. Found: C 85.36 and H 7.38.

1.3.4 2,13-Dibromo-4,4,11,11-tetrakis(4-hexylphenyl)-4,11-dihydrothieno[2',3':4,5]phenaleno[2,1-*b*]thieno[2',3':4,5]phenaleno[1,2-*d*]furan (DTPF4-2Br)

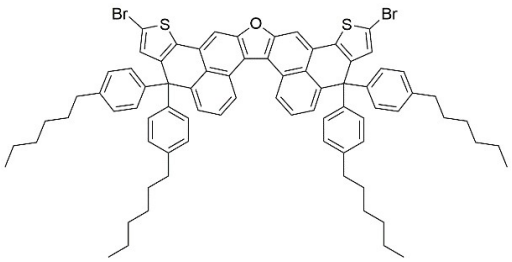

In a 100 mL round-bottom flask, **DTPF4** (2.20 g, 2.00 mmol) was dissolved in THF (40 mL). Subsequently, NBS (0.71 g, 4.00 mmol) was added, and the resulting mixture was stirred at room temperature for 1 hour. The reaction was then quenched with sodium sulfite aqueous solution. Water (50 mL) was added, and the resulting mixture was extracted three times with dichloromethane (3 × 100 mL). The organic phases were combined, washed with water, and dried over using anhydrous sodium sulfate. Upon removal of the solvent, the crude product was subjected to purification by column chromatography (eluent: toluene) on silica gel, yielding **DTPF4-2Br** as a yellow solid (2.49 g, 99% yield). Melting point: 184–185°C. ^{1}H NMR (500 MHz, THF-d_8) δ:

8.81 (d, J = 8.3 Hz, 2H), 7.82 (s, 2H), 7.51 (t, J = 7.9 Hz, 2H), 7.38 (d, J = 7.4 Hz, 2H), 7.11 (d, J = 8.6 Hz, 8H), 7.08 (d, J = 8.6 Hz, 8H), 6.86 (s, 2H), 2.59–2.52 (m, 8H), 1.63–1.54 (m, 8H), 1.38–1.25 (m, 24H), and 0.87 (t, J = 6.9 Hz, 12H) ppm. ^{13}C NMR (125 MHz, THF-d_8) δ: 155.64, 146.51, 146.42, 144.52, 142.15, 137.67, 134.18, 130.60, 129.52, 129.42, 128.99, 127.82, 127.07, 125.40, 125.19, 120.38, 112.58, 106.52, 59.33, 36.47, 32.85, 32.61, 30.28, 23.64, and 14.58 ppm. HR-MS (ESI) m/z calcd. for $([C_{78}H_{78}Br_2OS_2]^+Na)^+$: 1275.3753. Found: 1275.3768. ATR-FTIR (film) ν_{max} = 2953, 2923, 2853, 1584, 1507, 1456, 1321, 1193, 1059, 1021, 838, and 764 cm^{-1}. UV-vis (THF) λ_{max}: 408, 432, and 462 nm. Elemental analysis calcd. for $C_{78}H_{78}Br_2OS_2$: C 74.63 and H 6.26. Found: C 74.62 and H 6.28.

1.3.5 7,7'-(2,5-Bis(hexyloxy)-1,4-phenylene)bis(5-bromo-2,3-dihydrothieno[3,4-*b*][1,4]dioxine) (EBEH-2Br)

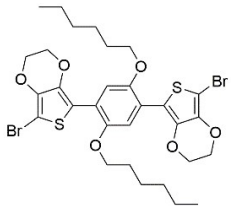

In a 100 mL round-bottom flask, **EBEH** (1.12 g, 2.00 mmol) was dissolved in THF (20 mL). After cooling to 0^{o}C, NBS (0.71 g, 4.00 mmol) was added, and the resulting mixture was stirred at 0^{o}C for 30 minutes. The reaction was then quenched with sodium sulfite aqueous solution. Water (50 mL) was added, and the resulting mixture was extracted three times with dichloromethane (3 × 100 mL). The organic phases were combined, washed with water, and dried over anhydrous sodium sulfate. Upon removal of the solvent, the crude product was purified by column chromatography (eluent: toluene) on silica gel, yielding **EBEH-2Br** as a milky white solid (1.42 g, 99% yield). ^{1}H NMR (500 MHz, THF-d_8) δ: 7.84 (s, 2H), 4.35–4.26 (m, 8H), 4.07 (t, J = 5.1 Hz, 4H), 1.94–1.85 (m, 4H), 1.57 (m, 4H), 1.44–1.35 (m, 8H), and 0.93 (t, J = 5.5 Hz, 6H) ppm. ^{13}C NMR (125 MHz, THF-d_8) δ: 149.53, 140.92, 139.39, 121.53, 114.48, 113.32, 88.50, 70.67, 66.04, 65.73, 32.75, 30.38, 27.06, 23.68, and 14.61 ppm. HR-MS (ESI) m/z calcd. for $([C_{30}H_{36}Br_2O_6S_2]^+H)^+$: 715.0393. Found: 715.0398. ATR-FTIR (film) ν_{max} = 2945, 2863, 1516, 1464, 1355, 1217, 1079, 1023, 917, 873, and 801 cm^{-1}. UV-vis (THF) λ_{max}: 313, 327, 374, and 391 nm. Elemental analysis calcd. for $C_{30}H_{36}Br_2O_6S_2$: C 50.29 and H 5.06. Found: C 50.27 and H 5.05.

1.3.6 p-DTPF4

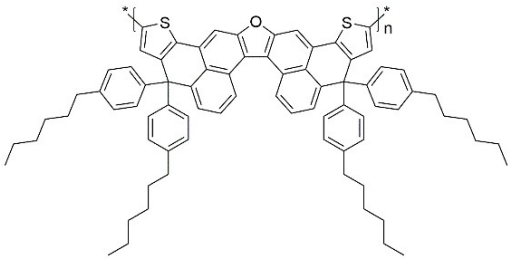

In a Schlenk reaction tube, **DTPF4** (0.55 g, 0.50 mmol), **DTPF4-2Br** (0.63 g, 0.50 mmol), $Pd_2(dba)_3$ (23 mg, 0.025 mmol), (*o*MeOPh)$_3$P (35 mg, 0.10 mmol), TMEDA (29 mg, 0.25 mmol), PivOH (0.26 g, 2.50 mmol), Cs_2CO_3 (0.49 g, 1.50 mmol), and toluene (10 mL) were combined. The reaction was stirred for 24 hours at 110°C under argon. Upon cooling to room temperature, the solvent was removed under vacuum, and methanol (20 mL) was introduced. The dark red solids were collected via filtration, followed by successive washing with a 0.1 M EDTA aqueous solution, water, and ethanol. The resultant residue underwent purification via a silica gel column, with elution performed sequentially using toluene/petroleum ether (*v*/*v*, 1/1) and toluene. The toluene fraction was collected, concentrated to a reduced volume, and then added dropwise into vigorously stirred methanol (100 mL). The resulting mixture was subjected to filtration, followed by drying, yielding the desired product as a dark red solid (0.47 g, 85%). Melting point: > 300°C. ^{1}H NMR (500 MHz, THF-d_8) δ: 8.93 (d, 2H), 7.99 (s, 2H), 7.78–7.55 (m, 2H), 7.42 (d, J = 8.5 Hz, 2H), 7.32–7.00 (m, 16H), 6.96 (s, 2H), 2.70–2.50 (m, 8H), 1.58 (m, 8H), 1.30 (m, 24H), and 0.87 (m, 12H) ppm. ATR-FTIR (film) ν_{max} = 2953, 2925, 2852, 1724, 1507, 1456, 1363, 1261, 1058, 1020, 803, 759, and 727 cm^{-1}. UV-vis (THF) λ_{max}: 572 nm. Elemental analysis calcd. for $(C_{78}H_{78}OS_2)_n$: C 85.51, H 7.18. Found: C 85.49, H 7.22.

1.3.7 p-DTPF4-EBEH

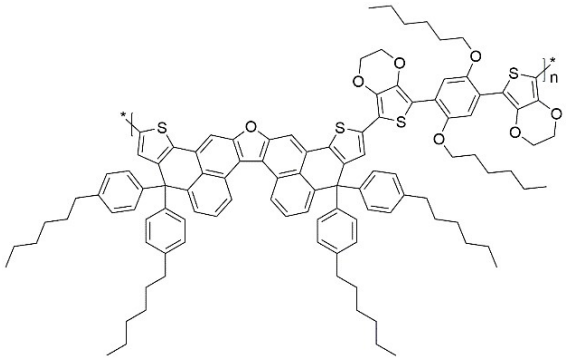

In a Schlenk reaction tube, **DTPF4-2Br** (0.63 g, 0.50 mmol), **EBEH** (0.28 g, 0.50 mmol), $Pd_2(dba)_3$ (23 mg, 0.025 mmol), (*o*MeOPh)$_3$P (35 mg, 0.10 mmol), TMEDA (29 mg, 0.25 mmol), PivOH (0.26 g, 2.50 mmol), Cs_2CO_3 (0.49 g, 1.50 mmol), and toluene (10 mL) were combined. The reaction was stirred for 24 hours at 110°C under argon. Upon cooling to room temperature, the solvent was removed under vacuum, and methanol

(20 mL) was introduced. The red solids were collected via filtration, followed by successive washing with a 0.1 M EDTA aqueous solution, water, and ethanol. The resultant residue underwent purification via a silica gel column, with elution performed sequentially using toluene/petroleum ether (*v*/*v*, 1/1) and toluene. The toluene fraction was collected, concentrated to a reduced volume, and then added dropwise into vigorously stirred methanol (100 mL). The resulting mixture was subjected to filtration, followed by drying, yielding the desired product as a red solid (0.69 g, 83%). Melting point: > 300°C. ^{1}H NMR (500 MHz, THF-d_8) δ: 8.79 (m, 2H), 8.01–7.79 (m, 4H), 7.63–7.47 (m, 2H), 7.41 (m, 2H), 7.19 (m, 8H), 7.08 (m, 8H), 7.01–6.91 (m, 2H), 4.45–4.18 (m, 8H), 4.15–4.04 (m, 4H), 2.57 (m, 8H), 1.99–1.84 (m, 4H), 1.60 (m, 12H), 1.42 (m, 8H), 1.33 (m, 24H), 0.95 (m, 6H), and 0.87 (m, 12H) ppm. ATR-FTIR (film) ν_{max} = 2952, 2924, 2854, 1463, 1439, 1360, 1085, 1020, 843, and 761 cm^{-1}. UV-vis (THF) λ_{max}: 525 and 562 nm. Elemental analysis calcd. for $(C_{108}H_{114}O_7S_4)_n$: C 78.51 and H 6.95. Found: C 78.52, H 6.93.

1.3.8 p-EBEH

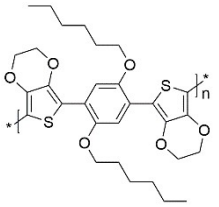

1.3.8.1 Palladium-catalyzed direct arylation polycondensation

In a Schlenk reaction tube, **EBEH-2Br** (0.36 g, 0.50 mmol), **EBEH** (0.28 g, 0.50 mmol), $Pd_2(dba)_3$ (23 mg, 0.025 mmol), (oMeOPh)$_3$P (35 mg, 0.10 mmol), TMEDA (29 mg, 0.25 mmol), PivOH (0.26 g, 2.50 mmol), Cs_2CO_3 (0.49 g, 1.50 mmol), and toluene (10 mL) were combined. The reaction was stirred for 24 hours at 110°C under argon. Upon cooling to room temperature, the solvent was removed under vacuum, and methanol (20 mL) was introduced. The orange solids were collected via filtration, followed by successive washing with a 0.1 M EDTA aqueous solution, water, and ethanol. The resultant residue underwent purification via a silica gel column, with elution performed sequentially using toluene and toluene/THF (v/v, 1/1). The toluene/THF fraction was collected, concentrated to a reduced volume, and then added dropwise into vigorously stirred methanol (100 mL). The resulting mixture was subjected to filtration, followed by drying, yielding the desired product as an orange solid (0.41 g, 73%). Melting point: 219–220°C. ^{1}H NMR (500 MHz, THF-d_8) δ: 7.85 (m, 2H), 6.35 (s, 0.24H), 4.43–4.17 (m, 8H), 4.07 (t, J = 4.6 Hz, 4H), 2.03–1.83 (m, 4H), 1.69–1.54 (m, 4H), 1.40 (m, 8H), and 0.94 (t, J = 5.1 Hz, 6H) ppm. ATR-FTIR (film) ν_{max} = 2925, 2865, 1721, 1507, 1429, 1356, 1217,

1078, 1071, 1047, 1024, 905, 872, and 727 cm^{-1}. UV-vis (THF) λ_{max}: 447 and 472 nm. Elemental analysis calcd. for $(C_{30}H_{36}O_6S_2)_n$: C 64.72 and H 6.52. Found: C 64.71 and H 6.52.

1.3.8.2 Oxidative polymerization via $FeCl_3$

In a Schlenk reaction tube, **EBEH** (0.56 g, 1.00 mmol), $FeCl_3$ (0.68 g, 4.20 mmol), and chlorobenzene (10 mL) were introduced. The ensuing reaction was stirred for 30 minutes at room temperature under an argon atmosphere. The mixture was then gently transferred into methanol (50 mL). The suspended red solids were collected via filtration, followed by successive washing with a 0.1 M EDTA aqueous solution, water, and ethanol. The resultant residue was almost insoluble in common organic solvents such as toluene, THF, and chlorobenzene.

1.4 Cyclic voltammetry measurements

A 10 μL solution of conjugated polymer in chlorobenzene, with a concentration of 5 mg mL^{-1}, was drop-cast onto the pre-cleaned surface of a 3 mm diameter glassy carbon electrode and air-dried, resulting in a modified working electrode. The electrolytic cell consisted of the modified working electrode, an FTO counter electrode, and an Ag/AgCl (sat. KCl) reference electrode. EMITFSI (0.1 M in MeCN) served as the supporting electrolyte. Cyclic voltammograms were recorded using a CHI660C electrochemical workstation (CH Instruments), with the reference electrode calibrated relative to ferrocene. Scan rate: 50 mV s^{-1}.

1.5 Ultraviolet photoelectron spectroscopy (UPS) measurements

Indium-doped tin oxide (ITO) glass substrates (12 Ω sq^{-1}, 1.6 mm thickness) underwent sequential sonication in detergent, deionized water, acetone, and ethanol for 15 minutes each. Subsequently, UV-ozone treatment was applied to activate the surface for 15 minutes. A uniform layer of PEDOT:PSS was spin-coated at 3000 rpm for 30 seconds onto the prepared ITO substrate and annealed at 150°C for 30 minutes. After cooling to room temperature, an organic semiconductor layer was deposited via spin-coating at 3000 rpm for 30 seconds using a chlorobenzene solution containing either spiro-OMeTAD, p-DTPF4, p-DTPF4-EBEH, or p-EBEH dissolved at a concentration of 20 mg mL^{-1}. UPS spectra were recorded using an ESCALAB XI+ instrument (Thermo Fisher).

1.6 Hole density measurements

To quantify the hole density (p) of pristine organic semiconductors, we performed impedance spectroscopy measurements on metal-insulator-semiconductor (MIS) devices. The MIS device architecture consisted of layers of n^{++}-Si/SiO_2/p-BCB/organic semiconductor/Au. The p-BCB layer was formed through a spin-coating process at 4000 rpm for 30 seconds using a BCB chlorobenzene solution (1 mg mL^{-1}), followed by annealing at 250°C

for 1 hour. Subsequently, an organic semiconductor layer was spin-coated from a chlorobenzene solution containing 132 mM TBP and spiro-OMeTAD (65 mg mL^{-1}), p-DTPF4 (40 mg mL^{-1}), p-DTPF4-EBEH (40 mg mL^{-1}), or p-EBEH (40 mg mL^{-1}) at 3000 rpm for 30 seconds, followed by the thermal evaporation of gold contacts (approximately 100 nm). Impedance spectra were acquired using an Autolab PGSTAT302N electrochemical workstation, covering a wide frequency range (10 Hz–3 MHz) with a small perturbation of 20 mV. The capacitance (C) was calculated using the equation: $C = -\frac{1}{\omega}[\frac{Z''-\omega L_i}{(Z'-R_s)^2+(Z''-\omega L_i)^2}]$, where ω denotes the angular frequency, Z' and Z'' represent the real and imaginary components of impedance, R_s is the series resistance, and L_i denotes the parasitic inductance. The p value was extracted from the slope of the Mott-Schottky plot, given by: $p = \frac{2}{q\varepsilon_r\varepsilon_0 \frac{d(A/C)^2}{dV}}$, where q is the elementary charge, ε_r denotes the relative permittivity, ε_0 signifies the vacuum permittivity, and A represents the area of the MIS device.

The determination of p for an organic semiconductor film containing TBPHTFSI presented a challenge. To address this obstacle, we adopted a comparative approach based on the quadratic integral intensities of electron paramagnetic resonance (EPR) signals originating from organic semiconductor films with and without TBPHTFSI. The established p value for a pristine organic semiconductor film served as the reference for this estimation. To capture the EPR spectrum, we applied a chlorobenzene solution onto a 2 cm × 2 cm microslide using the drop-casting method, subsequently crushed the microslide, and transferred it into a borosilicate glass tube. The chlorobenzene solutions were formulated to contain spiro-OMeTAD (65 mg mL^{-1}), p-DTPF4 (40 mg mL^{-1}), p-DTPF4-EBEH (40 mg mL^{-1}), or p-EBEH (40 mg mL^{-1}), each in combination with 132 mM TBP and varying weight percentages of TBPHTFSI (0, 5, 10, or 15). EPR measurements were performed using a Bruker A300-10/12 spectrometer.

1.7 Direct-current conductivity measurements

The direct-current conductivities (σ) of both pristine and composite organic semiconductor layers, deposited onto interdigital gold electrodes comprising 119 channels, each with a channel length (L) of 1.5 mm, a channel width (W) of 10 μm, and a channel thickness (t) of 110 nm, were determined by obtaining current–voltage (I–V) curves across potential biases ranging from −1.0 V to 1.0 V. The preparation of chlorobenzene solutions for depositing pristine and composite organic semiconductor layers is detailed in Section 1.6. Prior to measurement, the devices were stored in a dry air environment (< 5% relative humidity) for 7 days. I–V measurements were conducted using a Keithley 2400 source meter, with test automation facilitated by Labview 14.0. The

calculation of σ was performed using the formula $\sigma = sW/nLt$, where s represents the slope obtained from linear fitting of the I–V plot.

1.8 Young's modulus measurements

We determined the Young's modulus of organic semiconductor composites containing 15 wt% TBPHTFSI using the nanoindentation technique. The experiments were performed employing an iNano nanoindenter (KLA) equipped with a diamond Berkovich tip, characterized by an approximate tip radius of 20 nm, at room temperature. Prior to each test, meticulous calibration of the indenter's tip against fused silica was conducted, with adjustments made to ensure thermal drift remained well below 0.05 nm s^{-1}. The loading protocol involved a 10-second loading phase followed by a 10-second unloading phase. Specifically, the organic semiconductor composite film, deposited on quartz substrates, experienced an applied load of 0.5 mN. Throughout the entire testing procedure, the applied force and indentation depth into the samples were continuously monitored by the computer system. The determination of Young's modulus was accomplished by fitting the unloading curve of each sample using the widely accepted Oliver-Pharr method.[5]

1.9 Time-resolved photoluminescence measurements and sample preparation

The glass slides underwent sequential sonication in detergent, deionized water, acetone, and ethanol for 15 minutes each. Following cleaning, the glass slides were treated with UV-ozone for 15 minutes and then transferred into a glove box filled with dry air (< 3% relative humidity). The fabrication of the $FAPbI_3$ perovskite layer involved a two-step spin-coating process. Initially, a solution containing 1.5 M PbI_2 and 7.5 mM RbCl in a DMF:DMSO solvent mixture (9:1 volume ratio) was spin-coated onto the cleaned glass slides at 1500 rpm for 30 seconds, followed by annealing at 70°C for 1 minute. Subsequently, a solution mixture of FAI:MACl (90 mg:13.5 mg in 1 mL IPA) was spin-coated onto the PbI_2 layer at 1800 rpm for 30 seconds. The resulting film was annealed at 150°C for 30 minutes, resulting in the formation of the $FAPbI_3$ perovskite layer, incorporating a minor quantity of $(PbI_2)_2RbCl$.[6] For the passivation layer, a TTI-derived interlayer (2.5 mg mL^{-1} in chlorobenzene) was spin-coated at 5000 rpm for 30 seconds and annealed at 85°C for 20 minutes.[7] Subsequently, a chlorobenzene solution was spin-coated at 5000 rpm for 30 seconds. The chlorobenzene solution used for the deposition of the hole transport layer and control layer contained spiro-OMeTAD (65 mg mL^{-1}), p-DTPF4 (40 mg mL^{-1}), p-DTPF4-EBEH (40 mg mL^{-1}), p-EBEH (40 mg mL^{-1}), polystyrene (40 mg mL^{-1}), each in conjunction with 15 wt% TBPHTFSI and 132 mM TBP. Finally, a gold electrode (~ 100 nm) was deposited using a shadow mask under a vacuum of $\leq 1 \times 10^{-4}$ Pa. The resulting sample was covered with waterproof adhesive tape, further sealed with an epoxy adhesive (3M) on the gold electrode side, and stored in

dry air overnight. Time-resolved photoluminescence decay measurements were conducted using a Life-Spec-II fluorescence spectrometer (Edinburgh Instruments).

1.10 Fabrication of perovskite solar cells

The cleaned ITO substrates underwent UV-ozone treatment for 15 minutes prior to use. A diluted SnO_2 colloid dispersion, with a deionized water ratio of 1:4, was then subjected to filtration through a 0.2 μm PTFE filter. Subsequently, this refined solution was spin-coated onto the pristine ITO substrate at 4000 rpm for 30 seconds, followed by annealing at 150°C for 30 minutes within an ambient air environment.[8] Following UV-ozone treatment, the glass/ITO/SnO_2 substrates were transferred into a glove box filled with dry air (<3% relative humidity) for the deposition of perovskite layer, TTI-derived interlayer, hole transport layer, and gold electrode as described in Section 1.9. The resulting device, with an active area of 0.10 cm^2 was laminated with a high-quality anti-reflective film on the glass side. For encapsulation, see Section 1.9.

1.11 Photocurrent−voltage and external quantum efficiency measurements

The current density−voltage characteristics were determined using a Keithley 2400 source meter, with test automation facilitated by LabVIEW 14.0. Incident illumination was provided by an LS1000-4S-AM solar simulator (Solar Light Company), delivering AM1.5G irradiation level at 100 mW cm^{-2}, the intensity of which was validated via calibration against a silicon solar cell. To precisely define the photoactive region, a black metal mask with an aperture area of 0.07 cm^2 was utilized. The devices underwent comprehensive examination through both reverse scans (1.2 V → −0.1 V, incrementing in 0.005 V steps) and forward scans (−0.1 V → 1.2 V, with the same incremental step), conducted at a scan rate of 50 mV s^{-1}. For external quantum efficiency (EQE) measurements, an Omni-λ300 monochromator (Zolix, China) and a 150 W xenon lamp (Zolix, China) was employed. The photocurrent data were recorded using a Keithley 2400 source meter. In quantifying the monochromatic light intensity, a Hamamatsu S1337-1010BQ silicon diode calibrated at the National Institute of Metrology, China, was employed.

1.12 Thermostability

To evaluate the dark storage stability at 85°C (ISOS-D-2), perovskite solar cells were placed in an FD56 oven (Binder) set to the specified temperature. The atmospheric humidity surrounding the oven ranged from 45% to 90%. Periodic *J–V* measurements were conducted under AM1.5G conditions to continually monitor the performance parameters.

1.13 Operational stability assessment

Maximum power point (MPP) tracking was conducted using a 16-channel photovoltaic tracking system from YH Electronic Equipment Business, coupled with the SLS-LED-80A solar simulator by Qingdao Solar Scientific Instrument High-tech Co., LTD. The experiment was performed in a nitrogen-filled glovebox to ensure controlled conditions. MPP data were gathered at 5-minute intervals utilizing the perturb and observe method.

1.14 Disassembly of cells

The disassembly process commenced with the meticulous removal of the epoxy adhesive and waterproof adhesive tape, resulting in partial detachment of the gold electrode. Subsequently, a layer of magic tape (Scotch, 3M) was affixed onto the residual gold layer. Upon careful removal of the magic tape, the gold layer was completely eradicated. In cases where required, the hole transport layers underwent additional cleansing through five cycles of dynamic spin-coating with chlorobenzene.

1.15 Microscopy measurements

Top-view surface morphology of a thin film was imaged using a SU-70 field emission scanning electron microscope (Hitachi). Fluorescence optical microscopy images were recorded employing an ECLIPSE Ti-U system (Nikon). The samples were fabricated as described in Section 1.10 and 1.14.

1.16 X-ray diffraction measurements

The X-ray diffraction measurements were collected with a SmartLab® X-ray diffractometer (Rigaku) operating at 7200 W power (40 kV, 180 mA) and utilizing Cu Kα radiation (λ = 0.154 nm). For grazing incidence, samples were measured at an incidence angle of 0.20° relative to the substrate plane, and the scan range was 2^{o}–30^{o} with an incremental step of 0.05°. The samples for the grazing incidence measurements was prepared as follows. First, monocrystalline silicon substrates (1 cm × 1 cm) underwent successive sonication in ethanol for a duration of 15 minutes to ensure thorough cleaning. After cleaning, the substrates underwent UV-ozone treatment for 15 minutes to achieve surface activation prior to utilization. A layer of conjugated polymer was deposited via spin-coating at 1000 rpm for 30 seconds, utilizing a chlorobenzene solution comprising 132 mM TBP along with either p-DTPF4 (40 mg mL^{-1}), p-DTPF4-EBEH (40 mg mL^{-1}), or p-EBEH (40 mg mL^{-1}).

1.17 Water contact angle and waterproof measurements

Following a 15-minute UV-ozone treatment, the cleaned glass slides were transferred into a glove box filled with dry air (< 3% relative humidity) for the deposition of the $FAPbI_3$ perovskite layer, TTI-derived interlayer, and hole transport layer, as outlined in Section 1.9. The prepared samples were left in dry air for 3 days. Subsequently, water droplets were meticulously dripped onto both the $FAPbI_3$ perovskite film and the films

covered with hole transport layers. The water contact angle was then assessed using a DropMeter™ A-100P contact angle meter (Maist Co. Ltd.), while polarized optical microscopy images were captured using an SDPTOP CX40P system. Additionally, the thickness of the hole transport layer was determined utilizing a D-500 stylus profilometer (KLA-Tencor).

2 Theoretical modeling

2.1 DFT calculation

The frontier molecular orbitals and energy levels were computationally determined using the Gaussian 16 program suite. spiro-OMeTAD was computed using the density functional theory method at the B3LYP 6-311G(d,p) level of theory. Meanwhile, the conjugated polymers were calculated employing the periodic boundary condition density functional theory method, also at the B3LYP 6-311G(d,p) level of theory. *n*-Hexyl in conjugated polymers is replaced by ethyl for enhanced computational efficiency.

2.2 Molecular dynamics simulation

Polymer chains with a molecular weight of approximately 10 kDa were constructed using the Build Polymer tool in Material Studio 8.0. Subsequently, cubic boxes with periodic boundaries were generated using the Amorphous Cell module, accommodating either 10 polymer chains or a combination of 10 polymer chains intertwined with TBPHTFSI molecules at a weight percentage of 15. Molecular dynamics simulations were conducted employing the COMPASS II force field. Glass transition temperature and diffusivity investigations were carried out using the FORCITE module in Materials Studio 8.0. Our simulation protocol initiated with an initial NVT simulation at 700 K using a Nose thermostat, followed by an NPT simulation at 700 K utilizing both a Nose thermostat and a Berendsen barostat. Subsequently, a stepwise cooling process from 700 K down to 200 K was performed, with NVT and NPT simulations executed at each temperature. Specific volumes were recorded upon full equilibration at each temperature. The theoretical glass transition temperature was determined by intersection analysis of linear fitting lines in the low and high temperature regimes. Furthermore, H_2O or FAI was introduced into the organic semiconductor-TBPHTFSI composites, and NVT and NPT simulations were conducted. The mean square displacements of recorded trajectories were analyzed to unveil theoretical diffusivities. The Sorption module in Materials Studio 8.0 facilitated a grand canonical Monte Carlo simulation to evaluate the adsorption isotherm, yielding the solubility of H_2O. Water permeability was subsequently determined. Additionally, Young's modulus and cohesive energy density were simulated using the FORCITE module.

3 Additional figures and tables

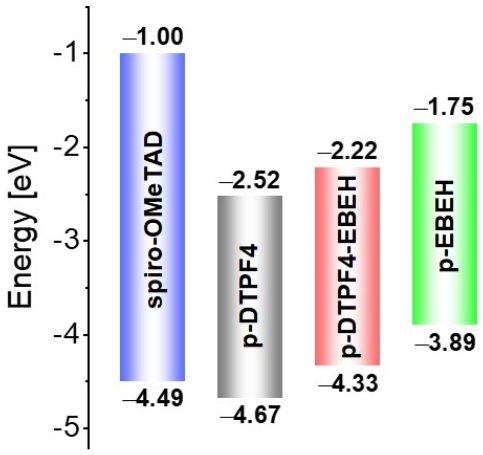

Fig. S1 DFT-calculated energy levels of frontier molecular orbitals. The HOMO and LUMO energy levels are indicated below and above the color bars, respectively.

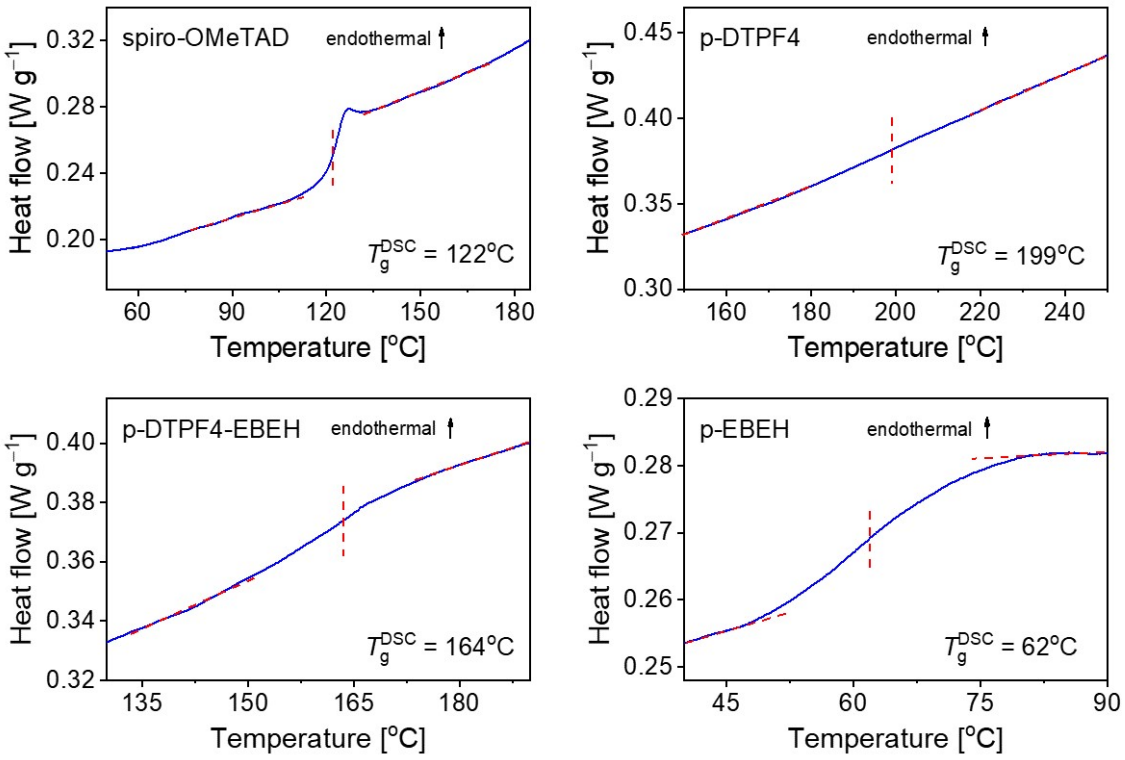

Fig. S2 Differential scanning calorimetry (DSC) thermograms of spiro-OMeTAD, p-DTPF4, p-DTPF4-EBEH, and p-EBEH. The glass transition temperatures (T_g^{DSC}) are also included. Note that for p-DTPF4, the glass transition measured by DSC is not very significant.

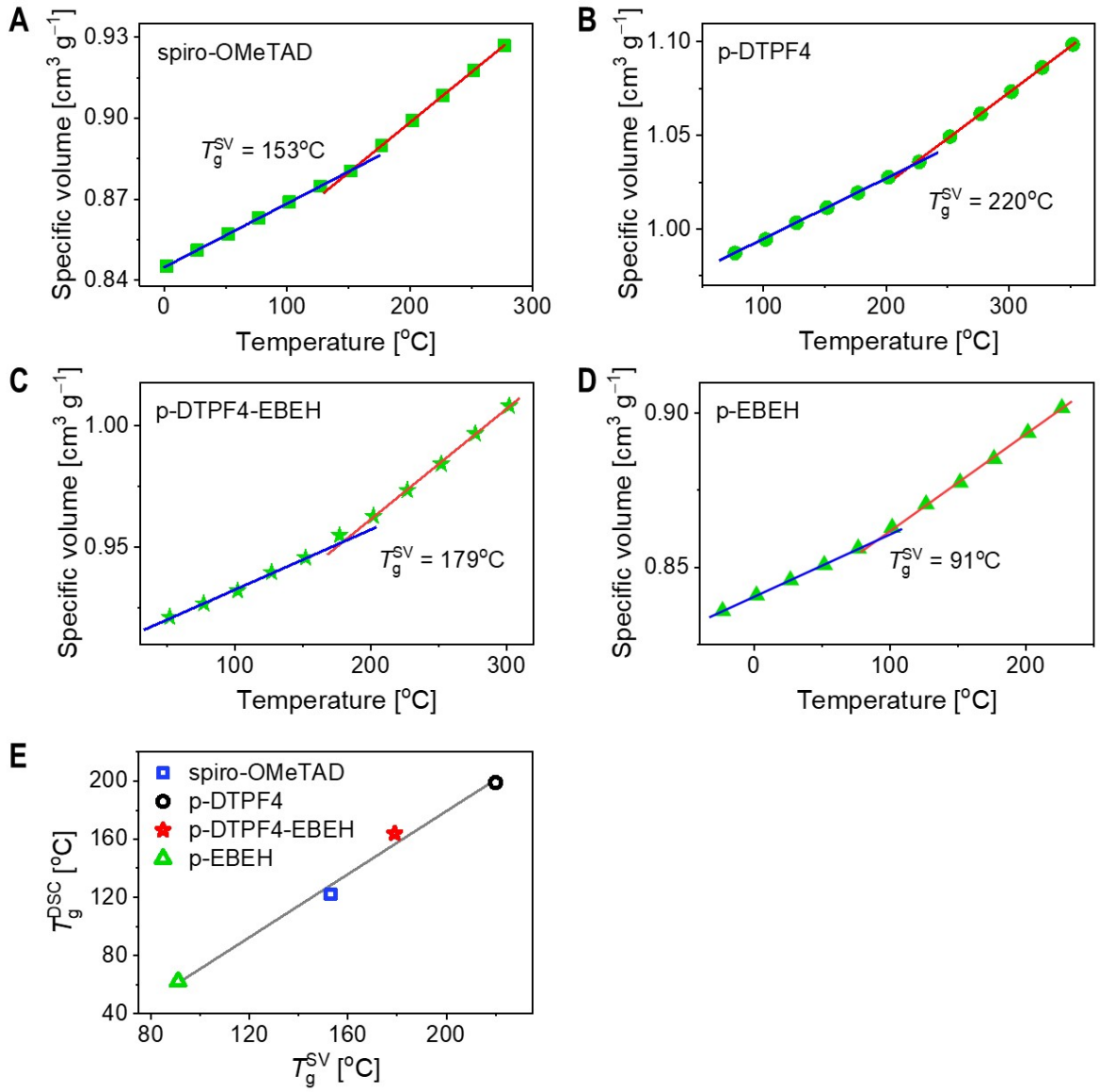

Fig. S3 (A–D) Plots illustrating the temperature-dependent behavior of specific volume. Linear regression analyses are employed to delineate distinct regimes—blue lines for the low-temperature domain and red lines for the high-temperature region. The intersection points of these linear fits unveil the specific volume-based glass transition temperature (T_g^{SV}). (E) Relationship between glass transition temperatures as determined by differential scanning calorimetry (T_g^{DSC}) and molecular dynamics simulation (T_g^{SV}).

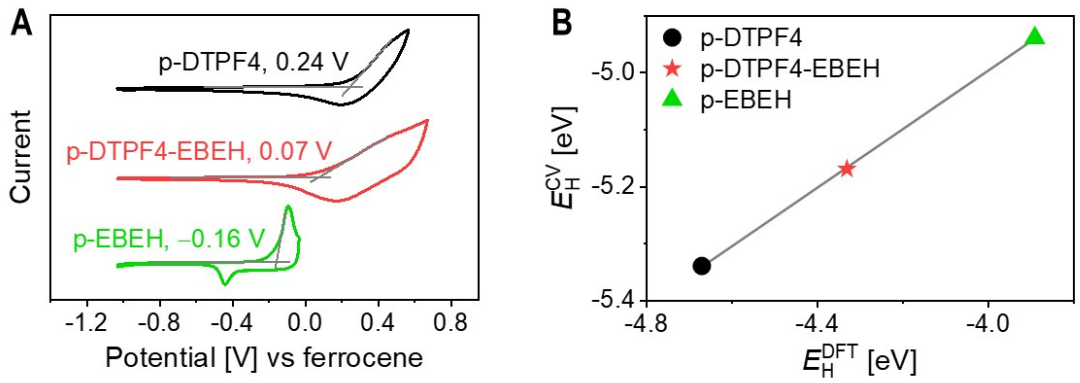

Fig. S4 (A) Cyclic voltammograms. The oxidation potential onset (V_{onset}, provided in the figure) was determined by identifying the intersection point between the tangent to the oxidation wave and the baseline aligned parallel to the *x*-axis. The HOMO energy levels (E_H^{CV}), derived from cyclic voltammograms, were calculated using the equation $E_H^{CV} = -5.10 - V_{onset}$,[9] where the E_H^{CV} values are –5.34 eV for p-DTPF4, –5.17 eV for p-DTPF4-EBEH, and –4.94 eV for p-EBEH, respectively. It is worth mentioning that a reliable cyclic voltammogram for a spiro-OMeTAD thin film could not be obtained using the same protocol. (B) Relationship between experimentally measured and theoretically calculated HOMO energy levels. E_H^{CV} denotes the values obtained from cyclic voltammetry measurements, while E_H^{DFT} denotes the values derived from theoretical calculations using the periodic boundary condition-density functional theory method.

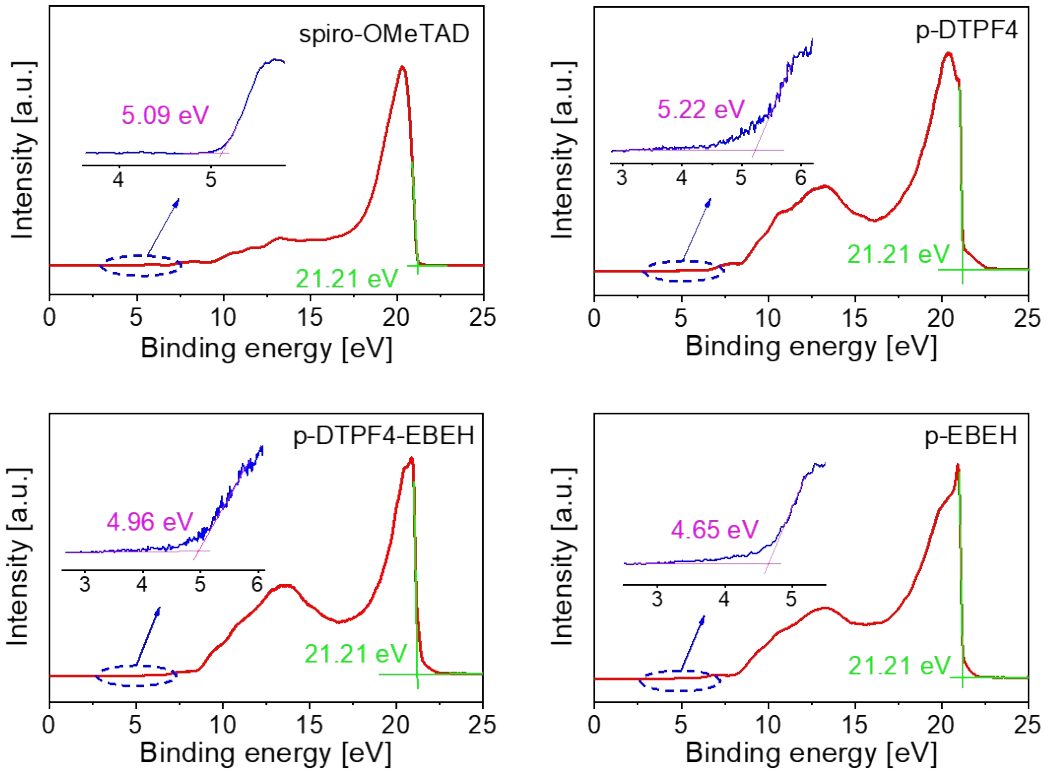

Fig. S5 Ultraviolet photoelectron spectra (UPS) depicting organic semiconductor thin films spin-coated onto the ITO/PEDOT:PSS substrate. These spectra have been calibrated to align their cutoff edges with the energy of He I photons (21.21 eV). The inset offers an enlarged view of the onset region. The determination of the HOMO energy level ($E_{\mathrm{H}}^{\mathrm{UPS}}$) relies on identifying the intersection point between the tangent to the spectrum in the low binding energy range and the baseline parallel to the *x*-axis.

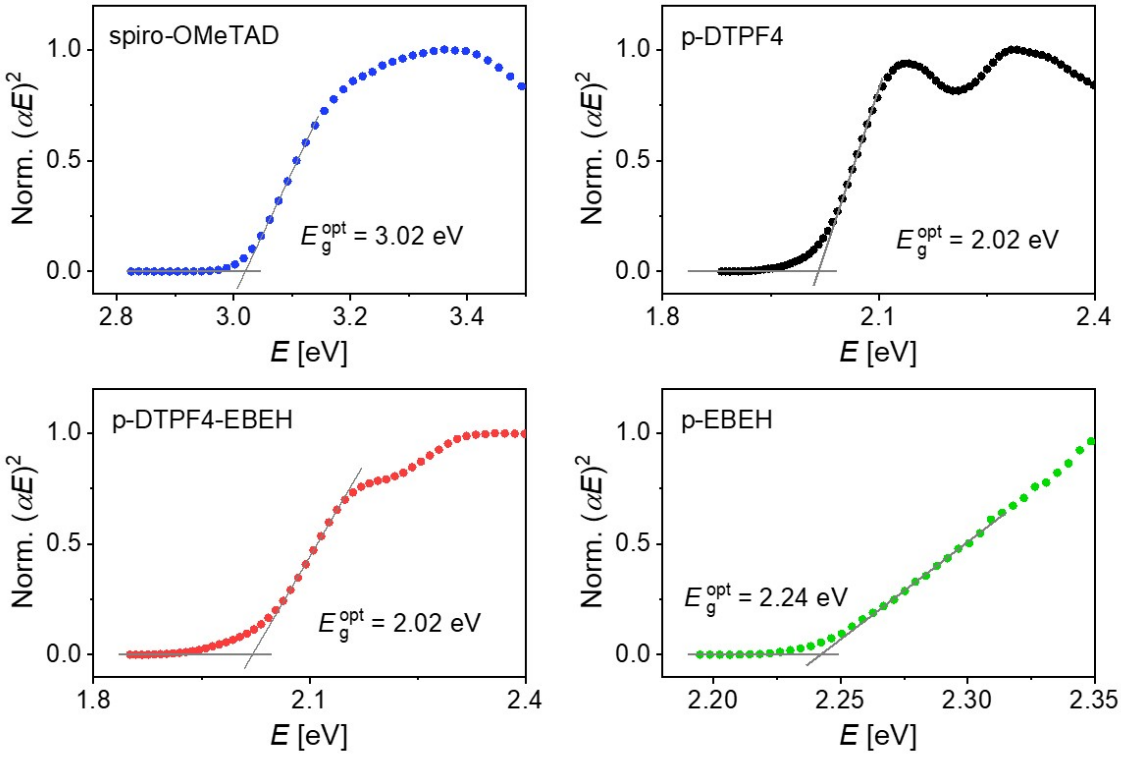

Fig. S6 Tauc plots illustrating organic semiconductor thin films on quartz substrate. E, α, and E_g^{opt} correspond to the photon energy, optical absorption coefficient, and optical bandgap, respectively. The determination of E_g^{opt} relies on identifying the intersection point between the tangent drawn to the spectral curve within the lower energy regime and the baseline, which runs in parallel to the *x*-axis.

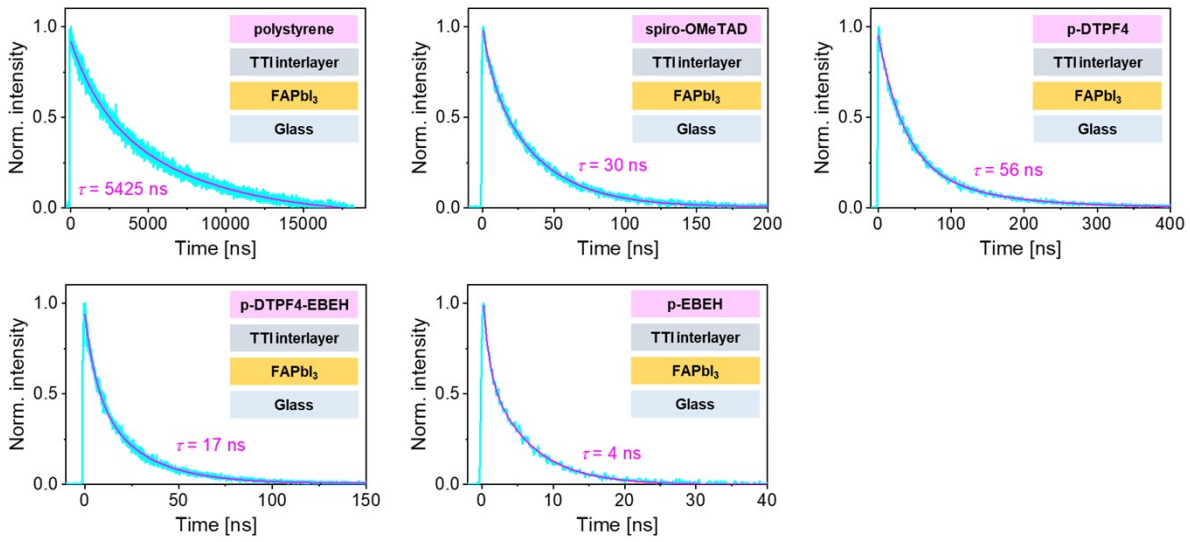

Fig. S7 Temporal evolution of the normalized intensity of photoluminescence in TTI-derived interlayer modified $FAPbI_3$ perovskite films, featuring organic coating layers with polystyrene or diverse organic semiconductors. The magenta curves correspond to biexponential decay fits, facilitating the extraction of the amplitude-weighted average photoluminescence lifetime (τ, included in the figure). Insets in each panel illustrate the layered architecture of the respective glass-supported film as utilized in the photoluminescence measurements. Excitation wavelength: 670 nm.

Table S1. Fitting parameters for photoluminescence decays in glass-supported $FAPbI_3$ films with diverse organic coating layers, amplitude-weighted average photoluminescence lifetimes, hole extraction rate constants, and hole extraction yields[a]

Organic coating layer	τ_1 [ns]	A_1	τ_2 [ns]	A_2	τ [ns]	k [10^7 s^{-1}]	ϕ_h [%]
polystyrene	1844	0.28	6817	0.72	5425	/	/
spiro-OMeTAD	7	0.21	36	0.79	30	0.033	99.4
p-DTPF4	34	0.69	104	0.31	56	0.018	99.0
p-DTPF4-EBEH	6	0.43	26	0.57	17	0.059	99.7
p-EBEH	1	0.38	6	0.62	4	0.250	99.9

[a] τ_1 and τ_2 represent the time constants of photoluminescence decay, A_1 and A_2 denote the relative amplitudes, and τ represents the amplitude-weighted average photoluminescence lifetime obtained by using equation $\tau = A_1\tau_1 + A_2\tau_2$. k represents the hole extraction rate constant obtained by using equation $k = \frac{\tau_P - \tau_H}{\tau_P \times \tau_H}$. ϕ_h represents the hole extraction yield obtained by using equation $\phi_h = \frac{\tau_P - \tau_H}{\tau_P}$, where τ_P represents amplitude-weighted average photoluminescence lifetime of the glass-supported $FAPbI_3$ film covered with polystyrene, and τ_H represents the amplitude-weighted average photoluminescence lifetime of the glass-supported $FAPbI_3$ film covered with hole transport layers.

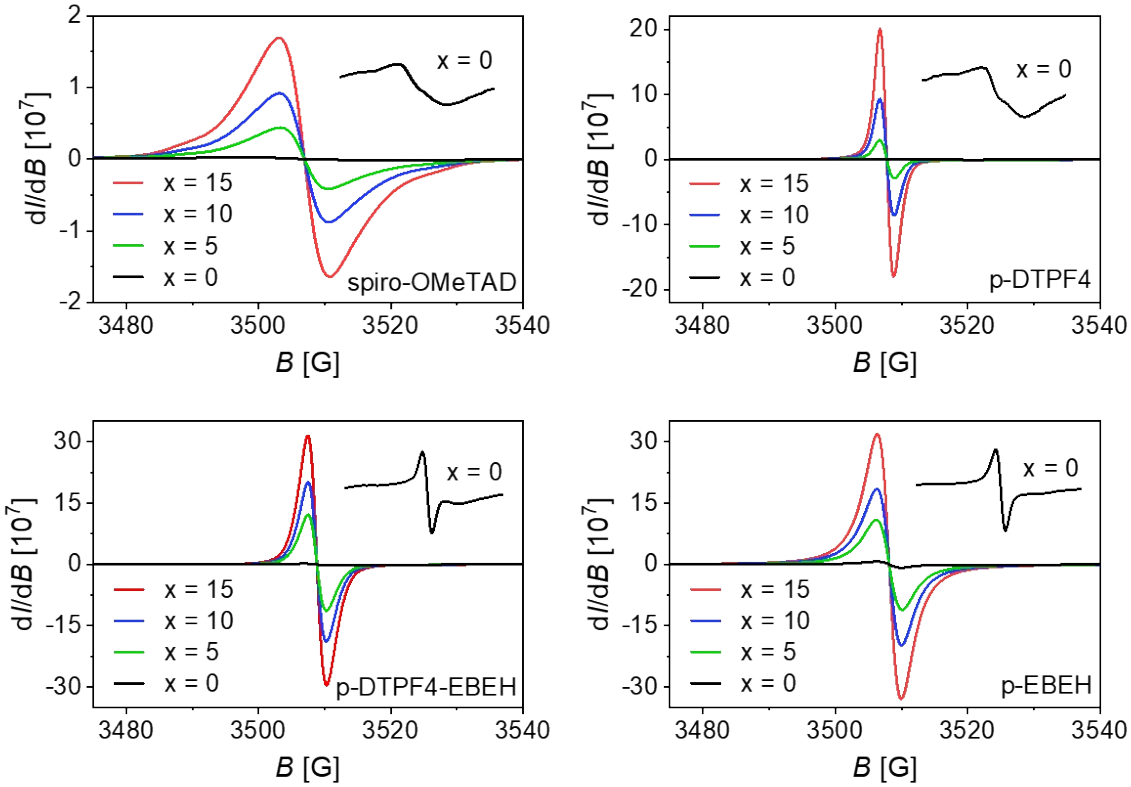

Fig. S8 Electron paramagnetic resonance (EPR) spectra of organic semiconductor films with varying weight percentages (x wt%) of TBPHTFSI, where the first derivative of absorption intensity (d*I*/d*B*) is plotted as a function of magnetic field strength (*B*). The insets show the enlarged spectra without TBPHTFSI. EPR signals are readily discernible in all organic semiconductor samples, even in the absence of TBPHTFSI, indicating the occurrence of unintentional doping, likely by atmospheric oxygen as a dopant, resulting in the formation of corresponding cationic radicals. We remark that TBPHTFSI functions as an oxygen doping promoter via ion-exchange rather than a dopant. As the TBPHTFSI content increases, EPR signals systematically intensify.

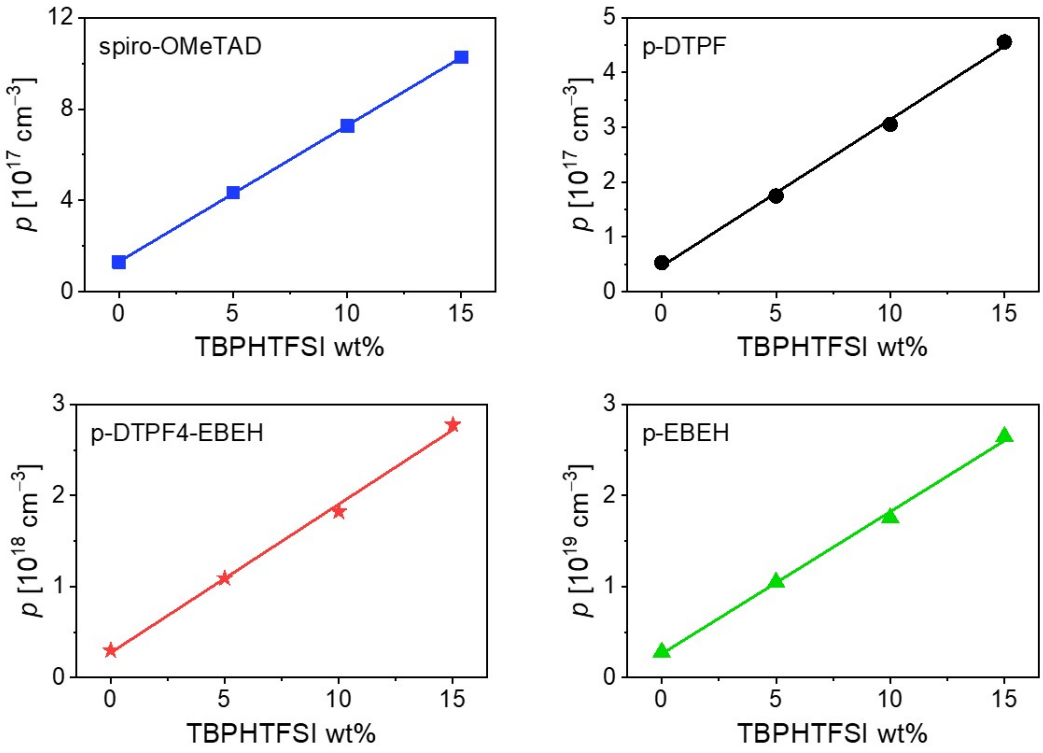

Fig. S9 Hole density (p) plotted as a function of TBPHTFSI weight percentage (wt%). Linear fits are represented by solid lines.

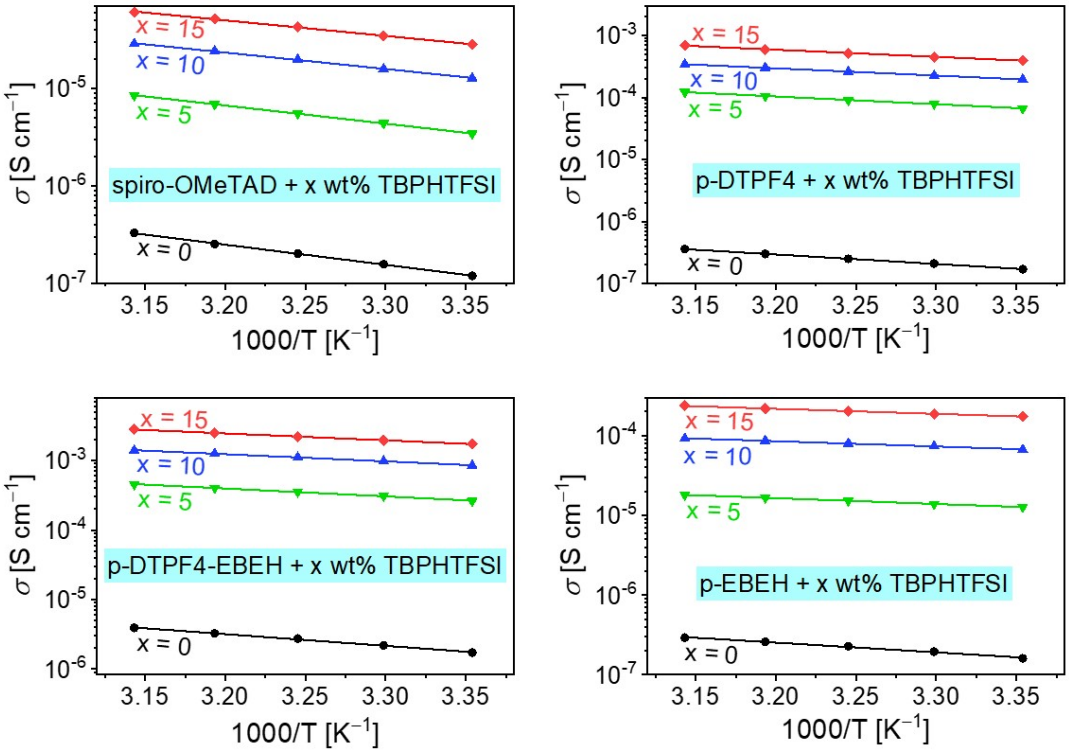

Fig. S10 Arrhenius plots depciting the temperature (T)-dependent electrical conductivity (σ) of organic semiconductor films at varying weight percentages (x wt%) of TBPHTFSI.

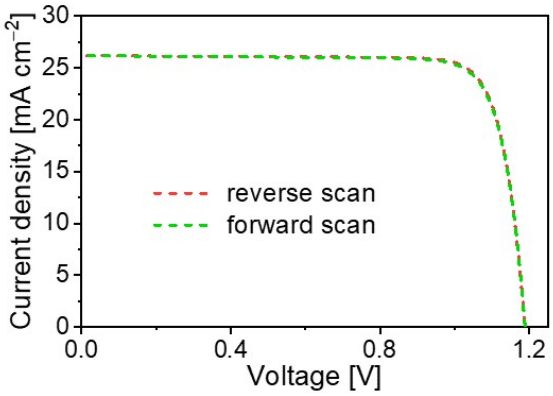

Fig. S11 Forward and reverse photocurrent density−voltage scans under simulated AM1.5G irradiation at 100 mW cm^{-2} for the representative as-prepared PSC with a p-DTPF4-EBEH-based hole transport layer containing 15 wt% TBPHTFSI.

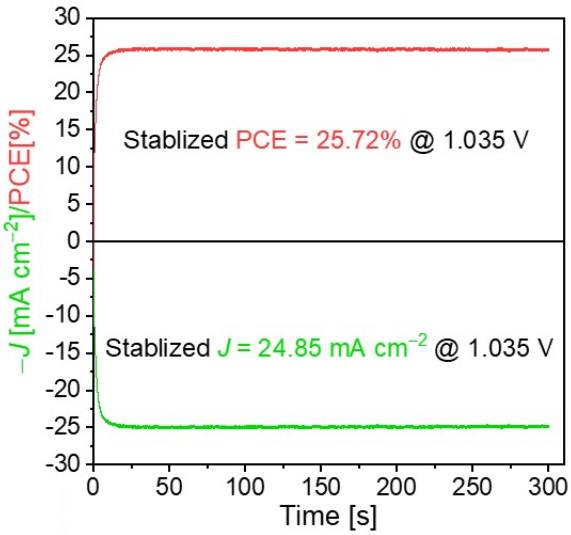

Fig. S12 Representative steady outputs of photocurrent density (*J*) and power conversion efficiency (PCE) under simulated AM1.5G irradiation at 100 mW cm^{-2} for the as-prepared PSC with a p-DTPF4-EBEH-based hole transport layer containing 15 wt% TBPHTFSI.

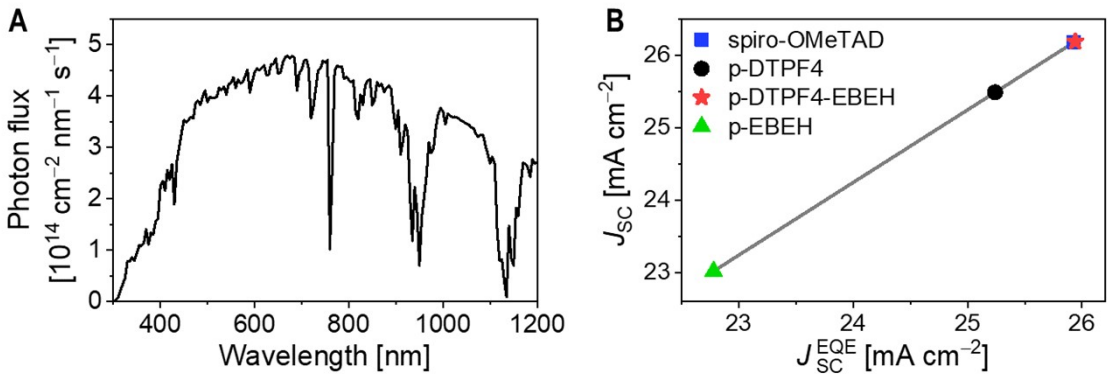

Fig. S13 (A) Photon flux of the AM1.5G solar spectrum (ASTM G173-03). (B) Relationship between short-circuit photocurrent density from photocurrent density−voltage measurements (J_{SC}) and photocurrent density derived from external quantum efficiency spectra (J_{SC}^{EQE}) for the as-prepared PSCs with different hole transporting layers. The gray line represents a linear fit.

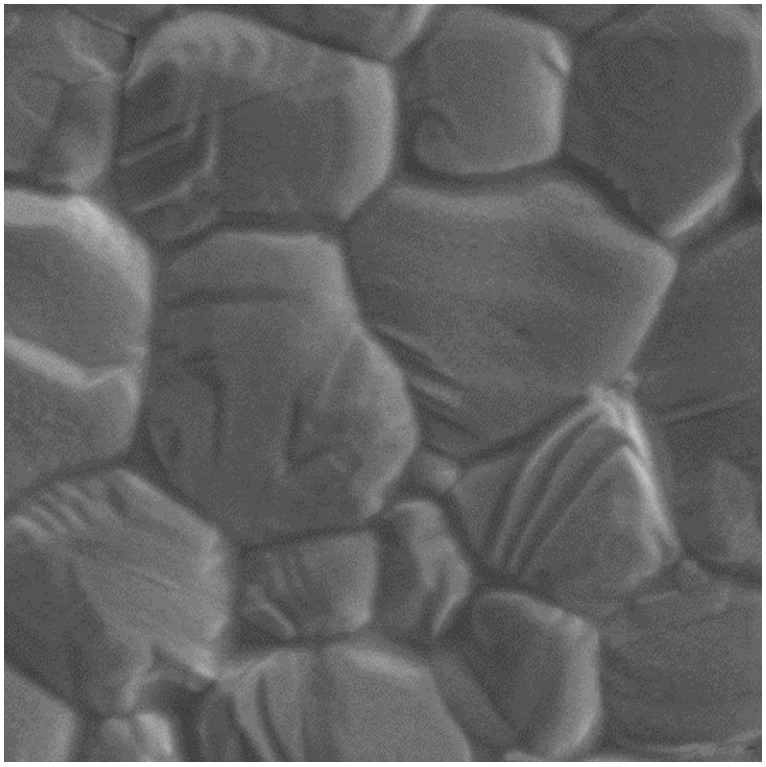

Fig. S14 Top-view scanning electron microscopy image of the TTI-modified $FAPbI_3$ perovskite layer in the as-prepared PSCs. Image dimensions: 4 μm × 4 μm. Prior to imaging, the encapsulation materials and the gold electrode covered on the hole transport layer were removed, and the hole transport layer was further washed away.

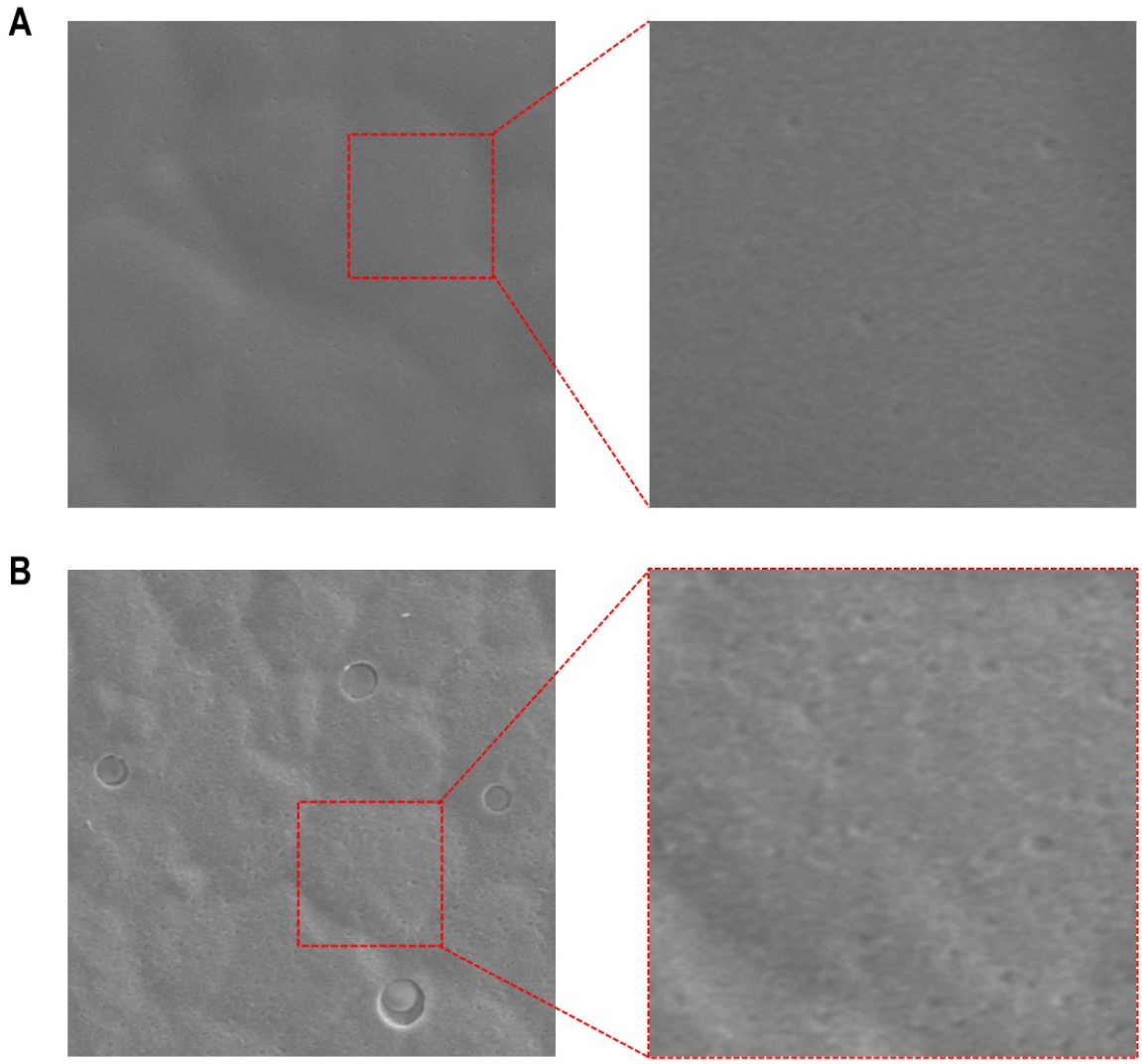

Fig. S15 Enlarged views of scanning electron microscopy images of the hole transport layers based on spiro-OMeTAD (A) and p-DTPF4 (B).

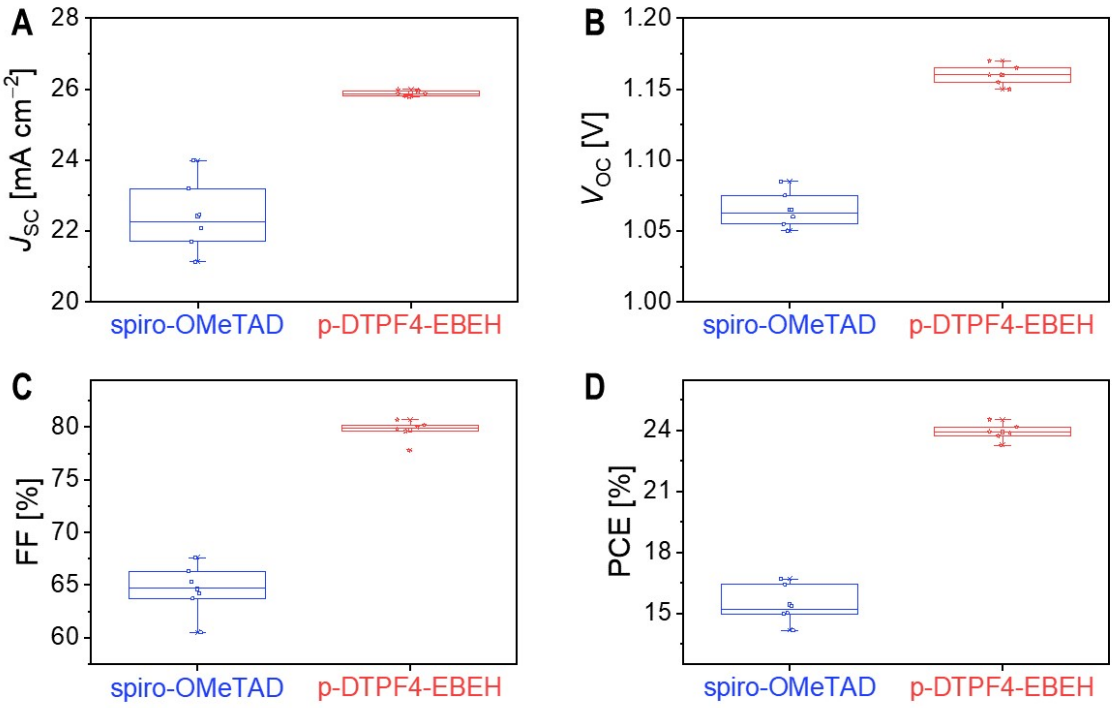

Fig. S16 Statistical analysis of photovoltaic parameters under simulated AM1.5G irradiation (100 mW cm^{-2}) for the 1000-hour, 85°C aged PSCs employing various hole transport layers containing 15 wt% TBPHTFSI: (A) short-circuit photocurrent density (J_{SC}); (B) open-circuit voltage (V_{OC}); (C) fill factor (FF); (D) power conversion efficiency (PCE).

Table S2. Representative photovoltaic parameters of PSCs with various hole transport layers after 1000-hour, 85°C aging

cell	J_{SC} [mA cm^{-2}]	V_{OC} [V]	FF [%]	PCE [%]	J_{SC}^{EQE} [mA cm^{-2}]
spiro-OMeTAD/aged	22.45	1.065	64.2	15.3	22.05
p-DTPF4-EBEH/aged	25.87	1.160	79.8	23.9	25.57

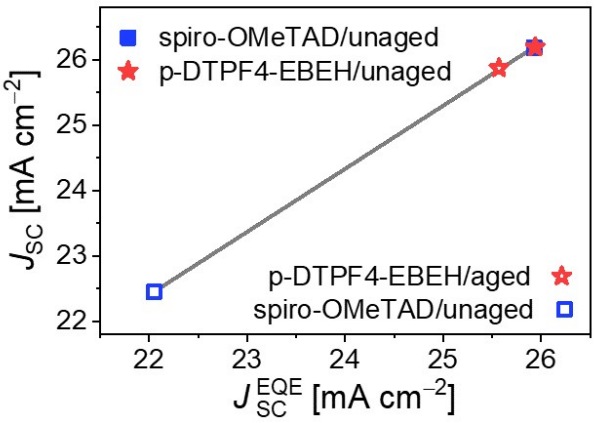

Fig. S17 The relationship between short-circuit photocurrent density derived from photocurrent density−voltage measurements (J_{SC}) and photocurrent density derived from external quantum efficiency spectra (J_{SC}^{EQE}) is illustrated for the unaged and 1000-hour, 85°C aged PSCs with different hole transporting layers. A linear fit is denoted by the gray line.

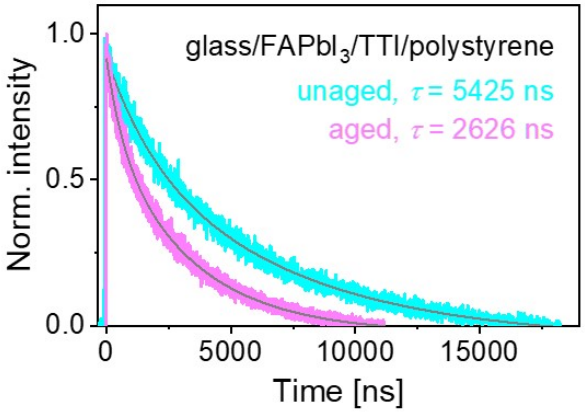

Fig. S18 Time-resolved photoluminescence traces at 810 nm for the dummy cell (glass/FAPbI$_3$/TTI-derived interlayer/polystyrene/gold) before and after 1,000-hour, 85°C aging. The excitation wavelength utilized was 670 nm.

Fig. S19 Fluorescence optical microscopy images of perovskite layers in as-prepared PSCs with hole transport layers containing 15 wt% TBPHTFSI. Image dimensions: 25 μm × 25 μm.

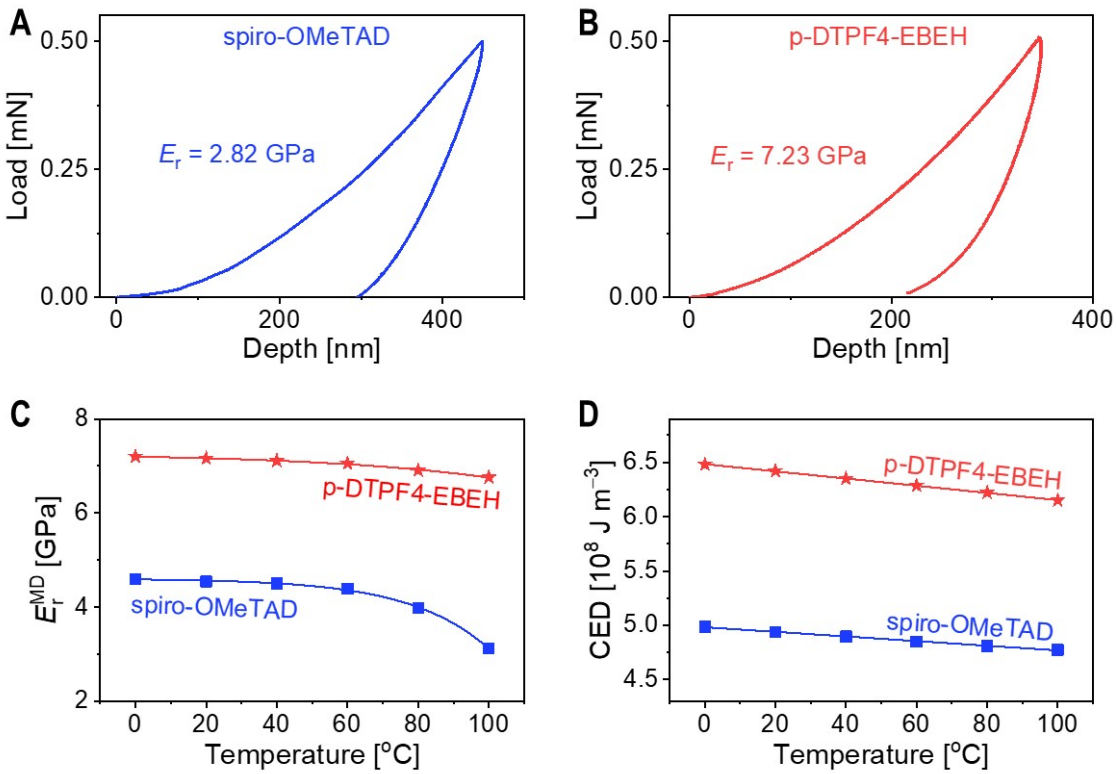

Fig. S20 Mechanical characterization of organic semiconductor composite thin films containing 15 wt% TBPHTFSI. (A and B) Nanoindentation curves depicting mechanical properties. The derived Young's modulus (E_r) is also presented. (C) Molecular dynamics (MD) simulated Young's modulus (E_r^{MD}) plotted against temperature. (D) MD simulated cohesive energy densities (CED) plotted against temperature.

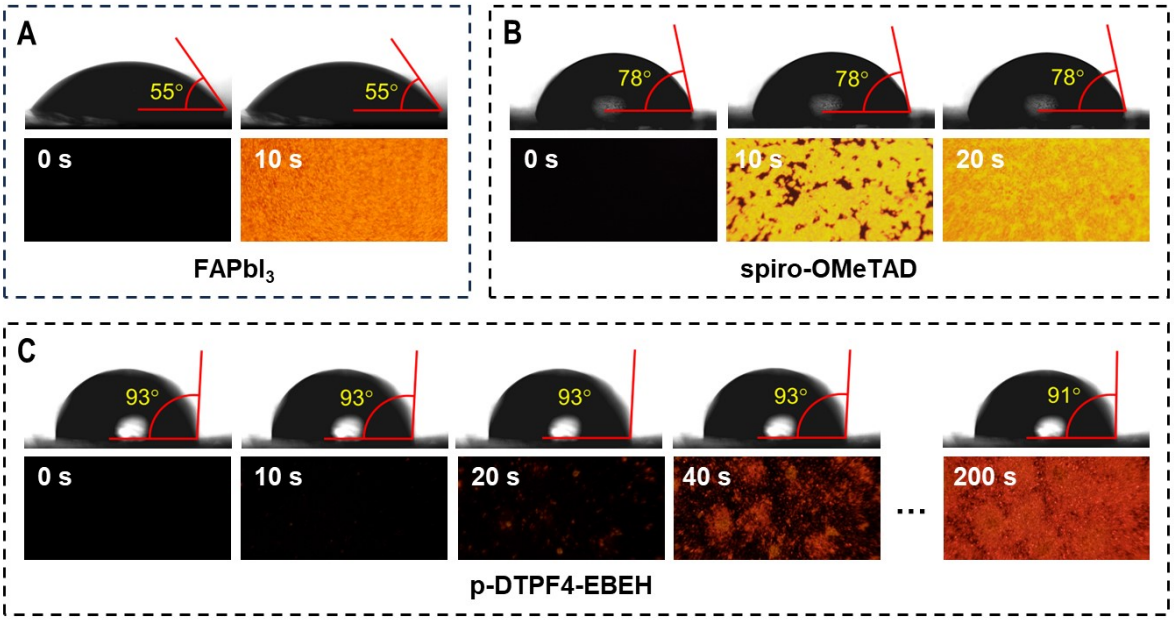

Fig. S21 Visualization of the waterproof ability of a hole transport layer. (A–C) Water contact angles and polarized optical microscopy images captured at various time intervals following the application of a water droplet onto the surface of the $FAPbI_3$ perovskite film (A) and the corresponding film covered with a hole transport layer (B and C). Image dimensions: 500 μm × 250 μm.

4 Appendix: ^{1}H NMR spectra, ^{13}C NMR spectra, mass spectra, infrared spectra, UV-vis spectra, and HT-GPC analyses

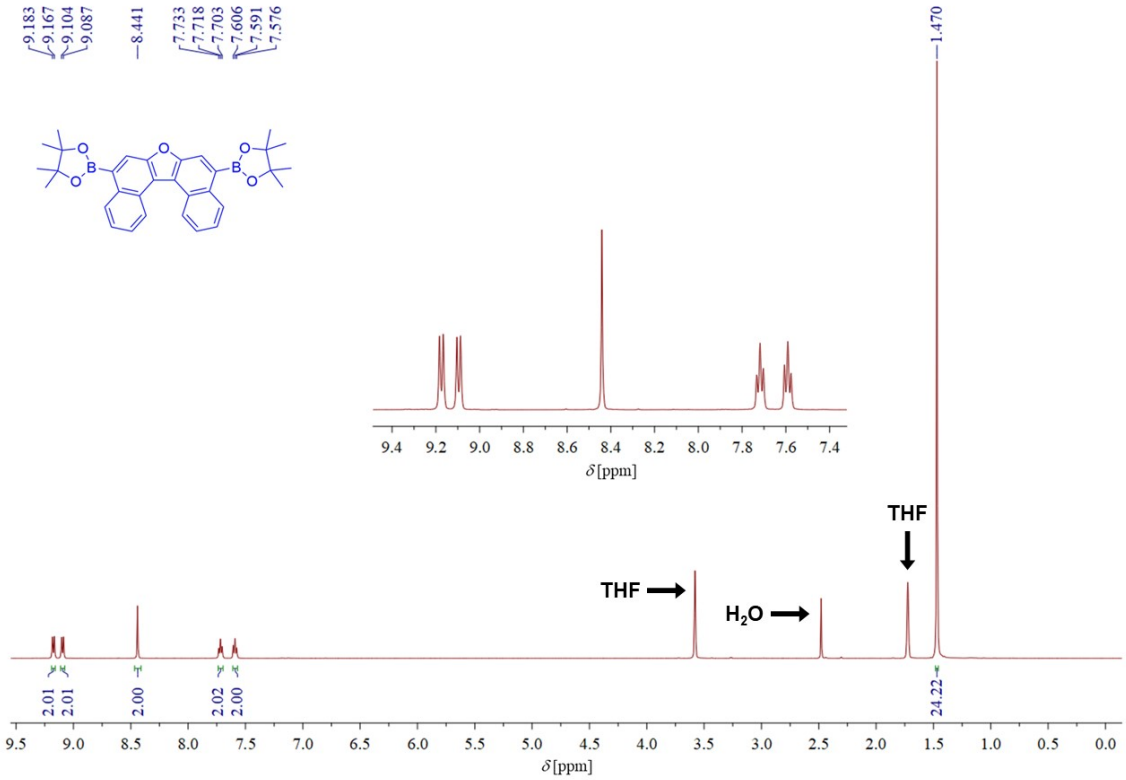

Fig. S22 ^{1}H NMR (500 MHz) spectrum of compound **2** in THF-d_8.

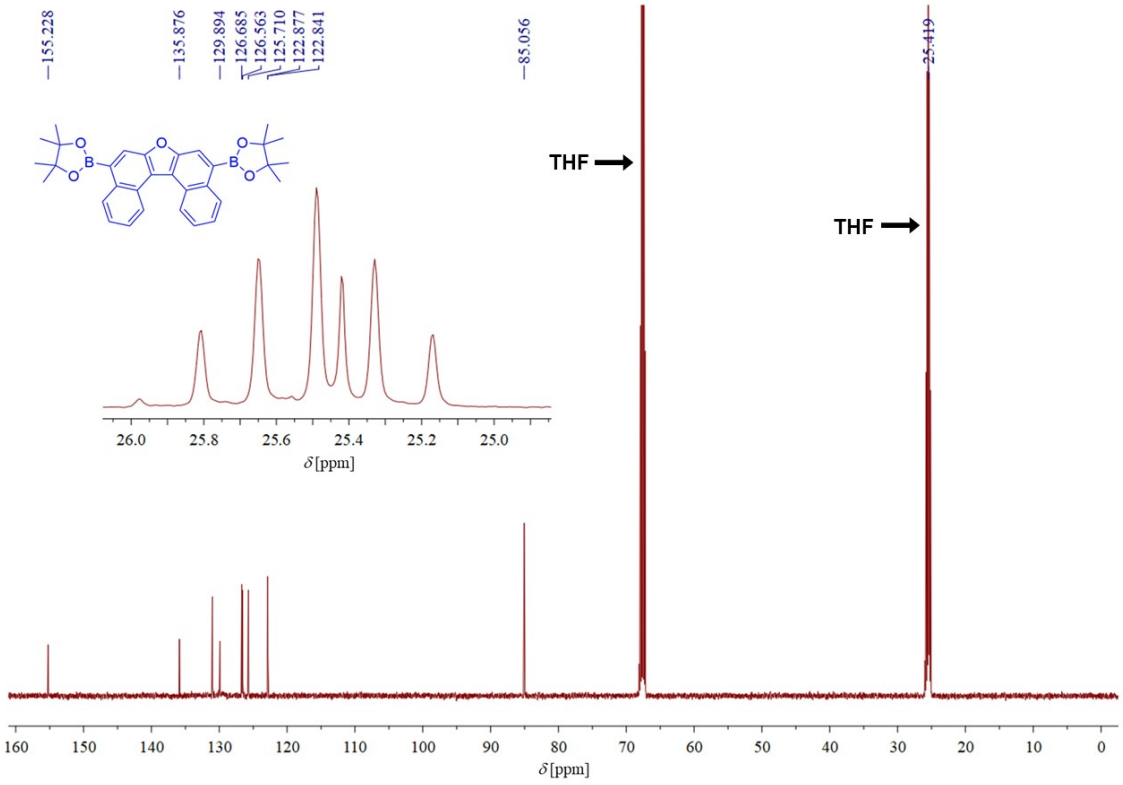

Fig. S23 ^{13}C NMR (125 MHz) spectrum of compound **2** in THF-d_8.

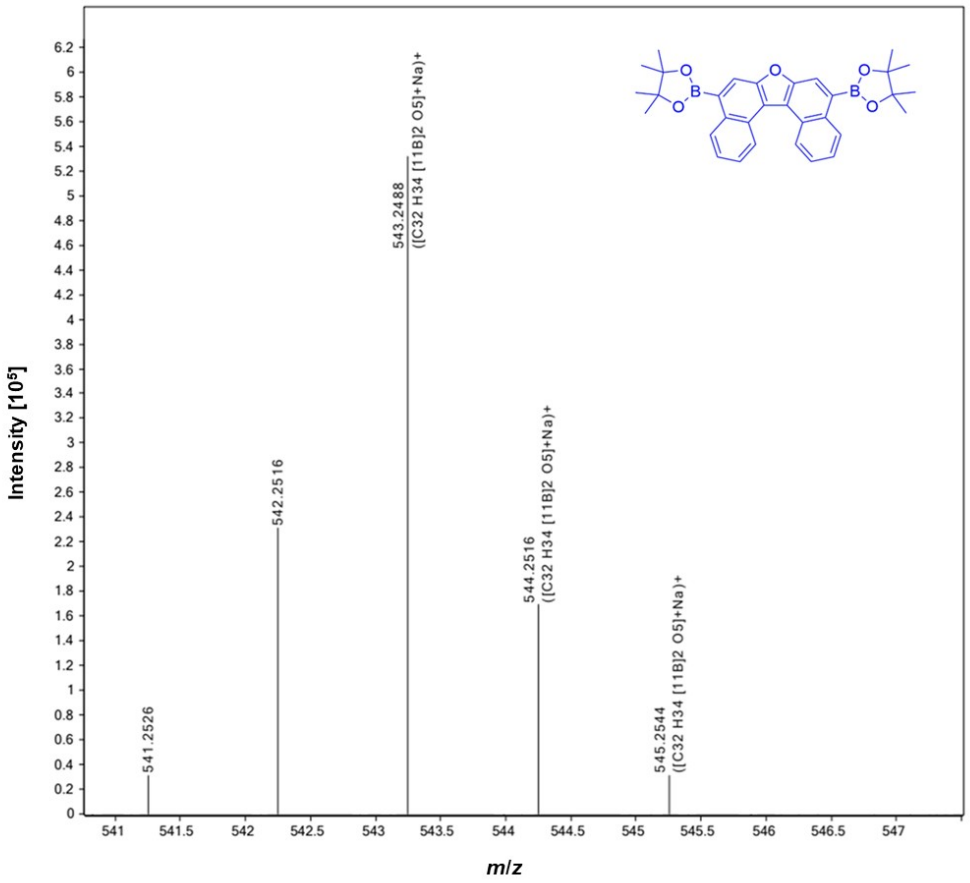

Fig. S24 High-resolution mass spectrum (ESI) of compound **2**.

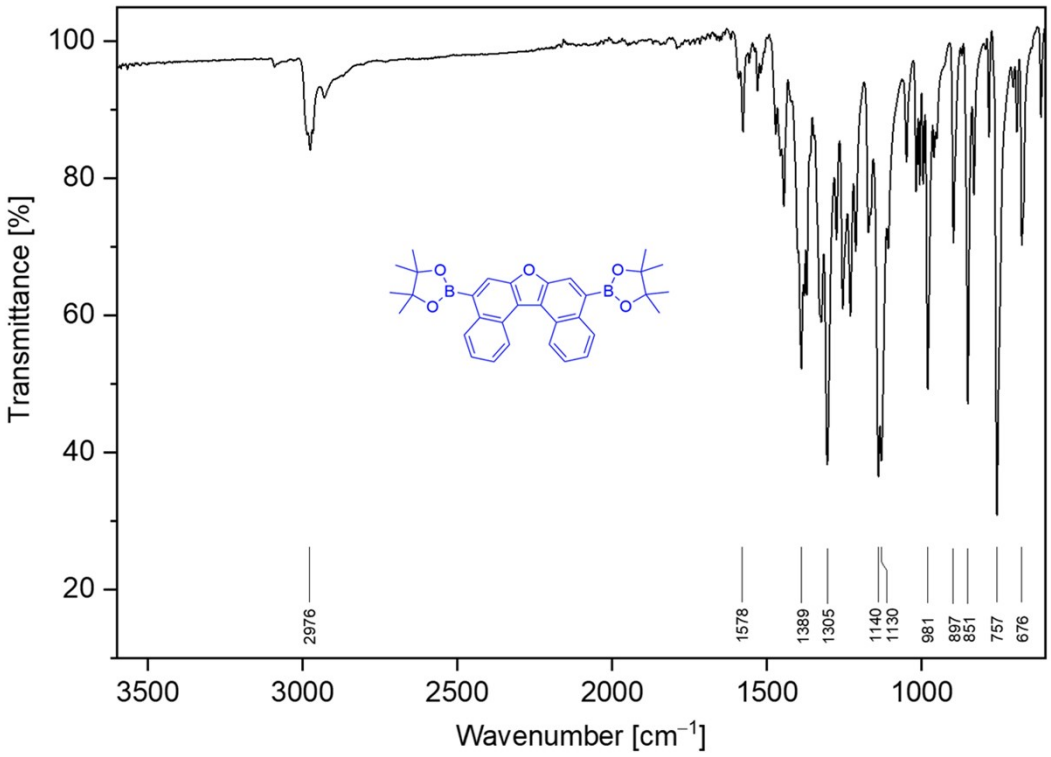

Fig. S25 ATR-FTIR spectrum of compound **2**.

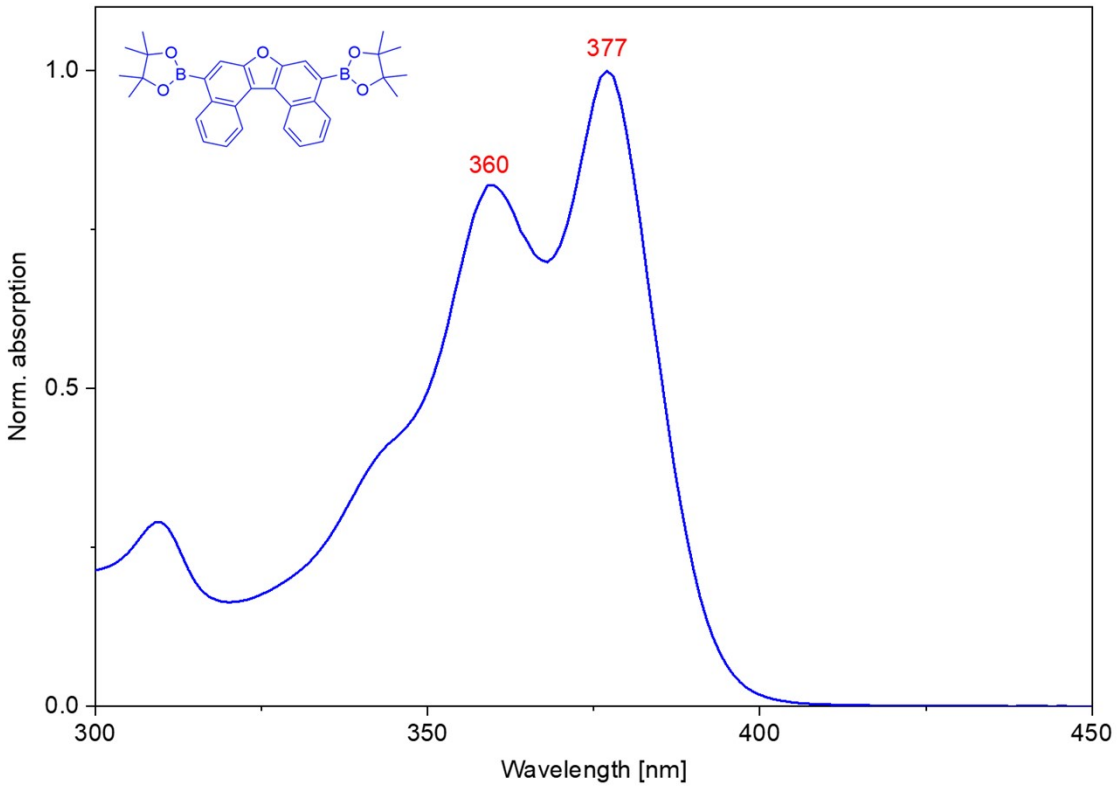

Fig. S26 UV-vis absorption spectrum of compound **2** in tetrahydrofuran.

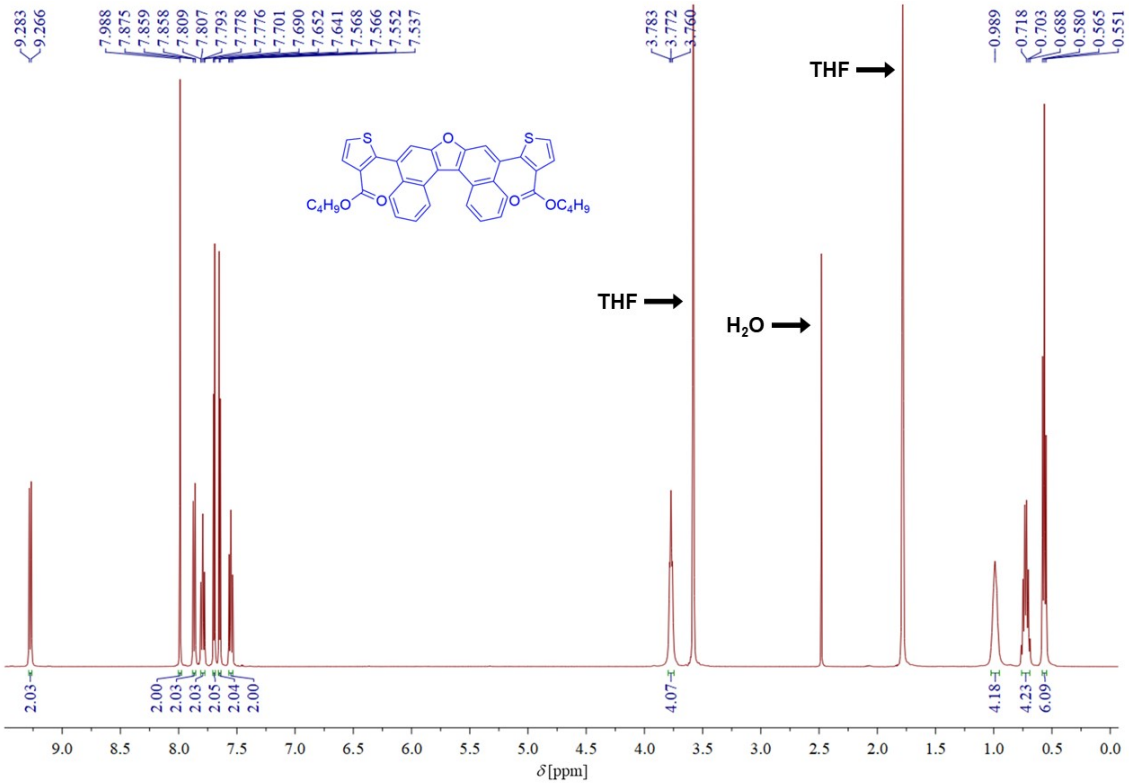

Fig. S27 ^{1}H NMR (500 MHz) spectrum of compound **3** in THF-d_8.

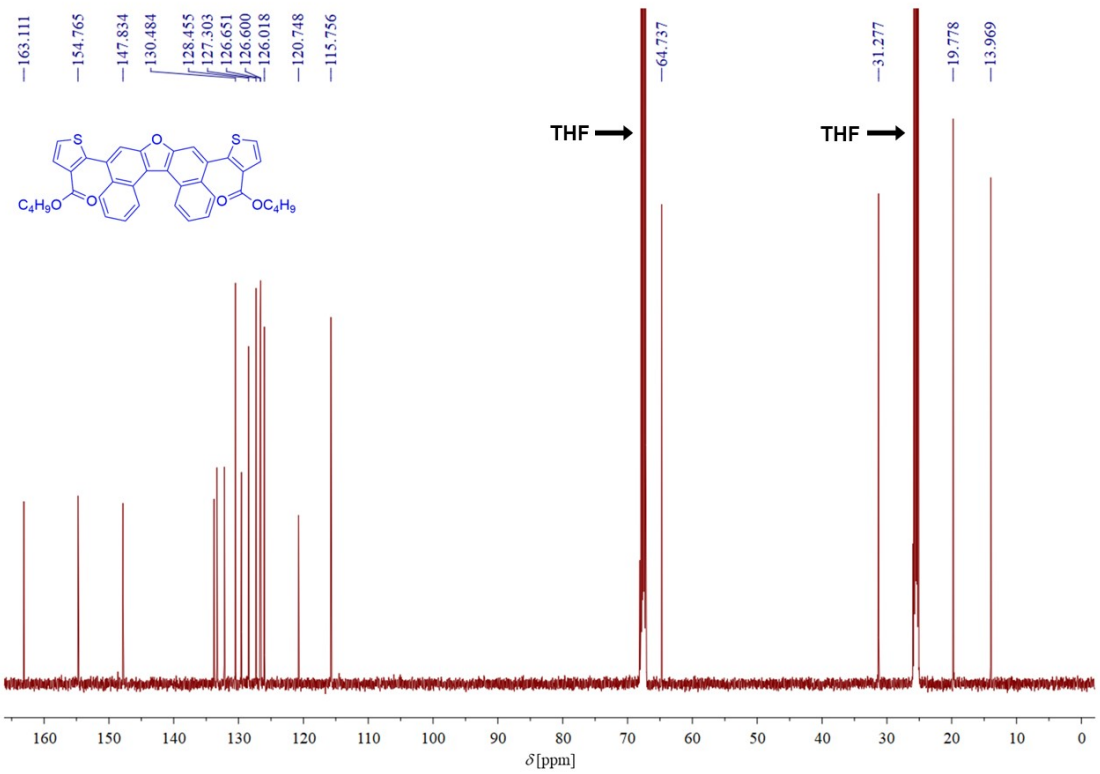

Fig. S28 ^{13}C NMR (125 MHz) spectrum of compound **3** in THF-d_8.

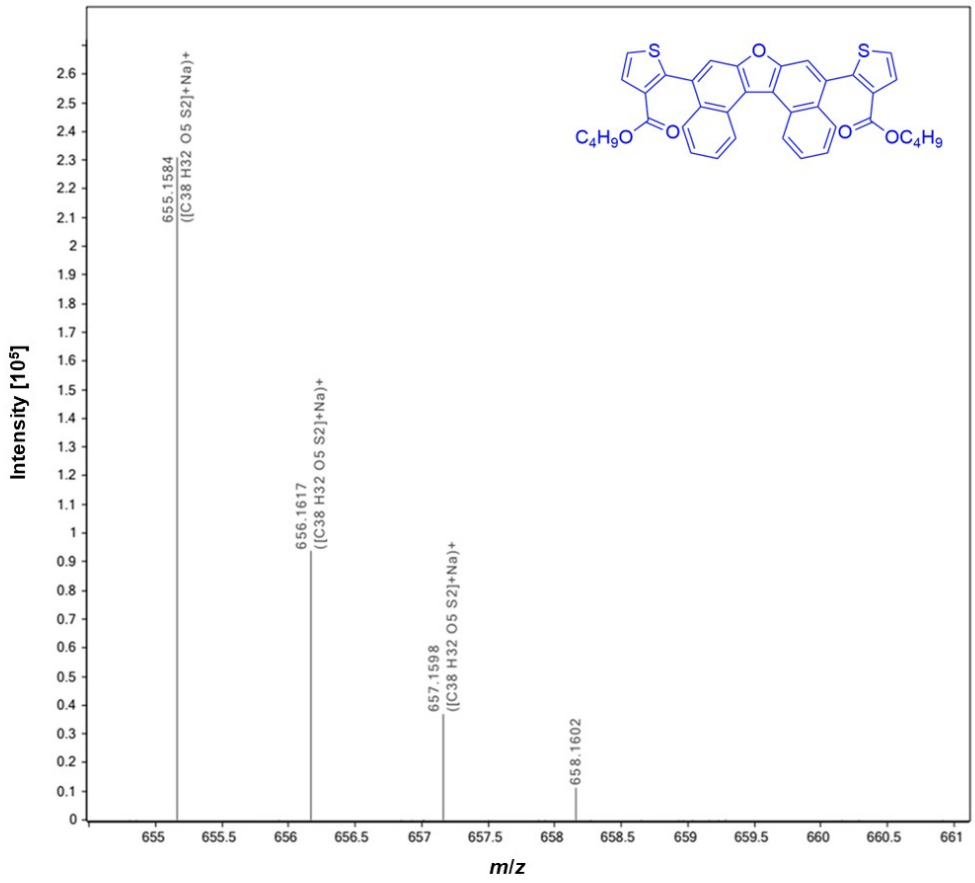

Fig. S29 High-resolution mass spectrum (ESI) of compound **3**.

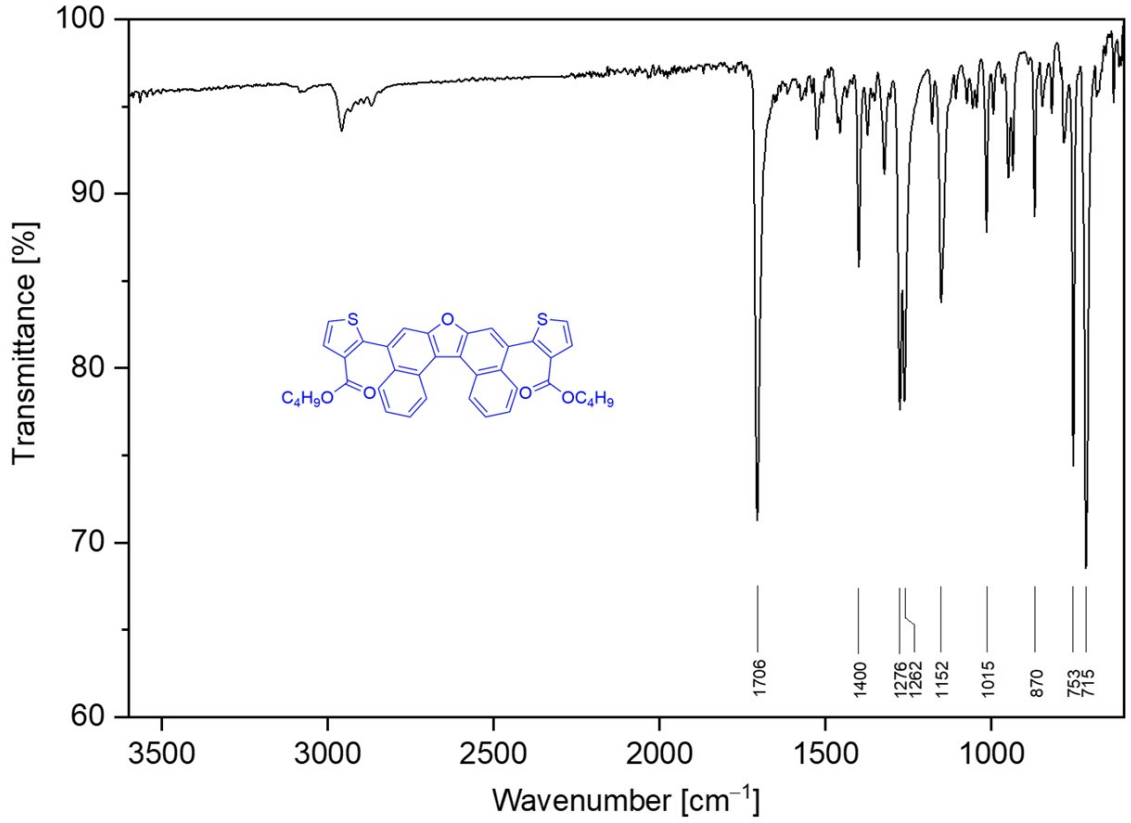

Fig. S30 ATR-FTIR spectrum of compound **3**.

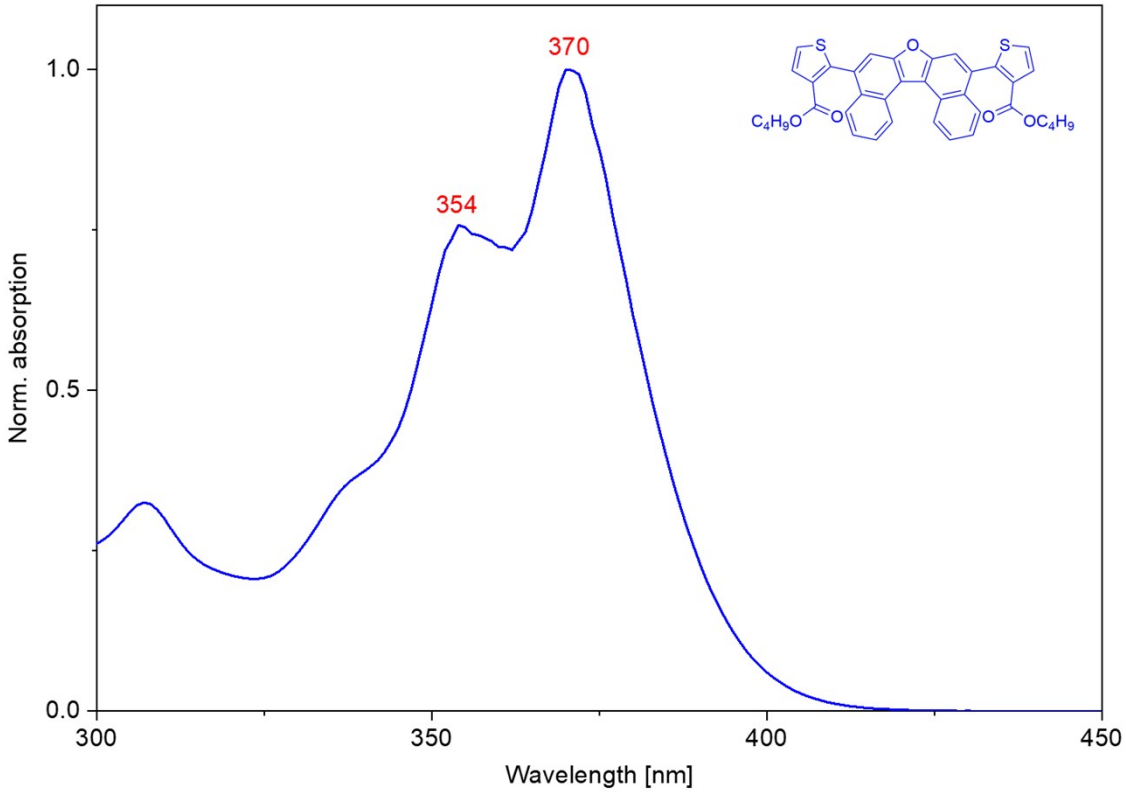

Fig. S31 UV-vis absorption spectrum of compound **3** in tetrahydrofuran.

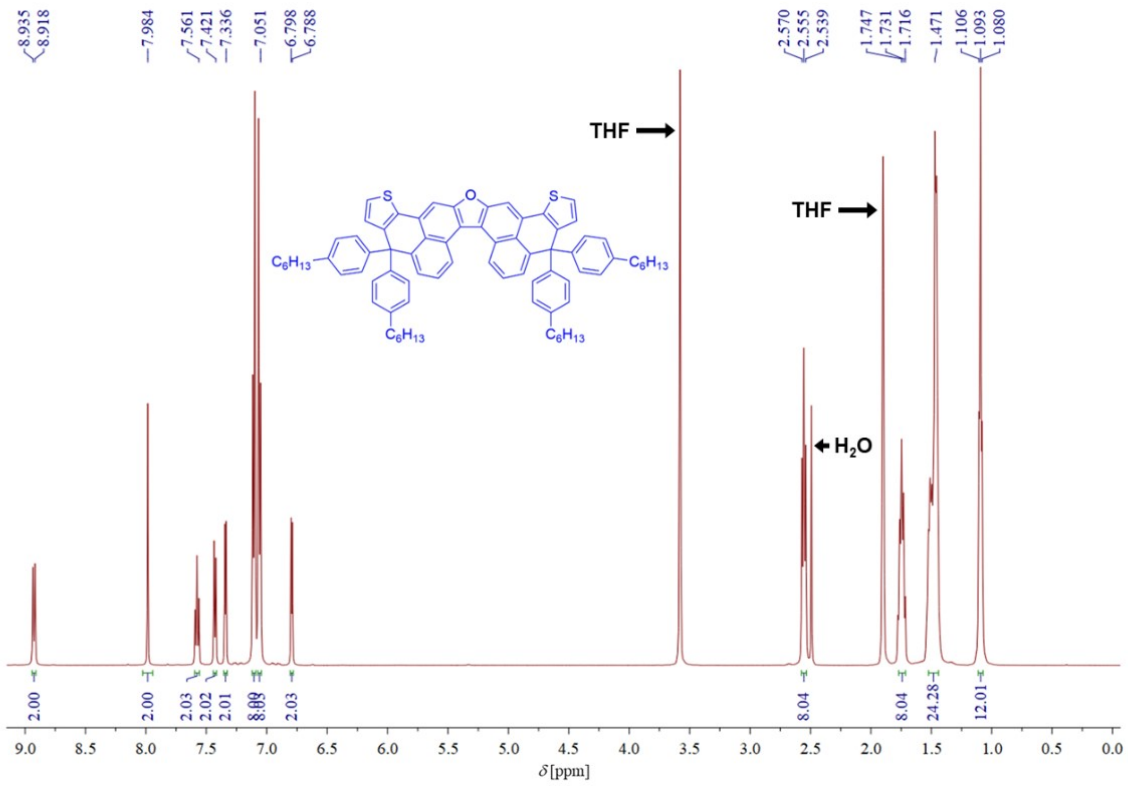

Fig. S32 [1]H NMR (500 MHz) spectrum of **DTPF4** in THF-d_8.

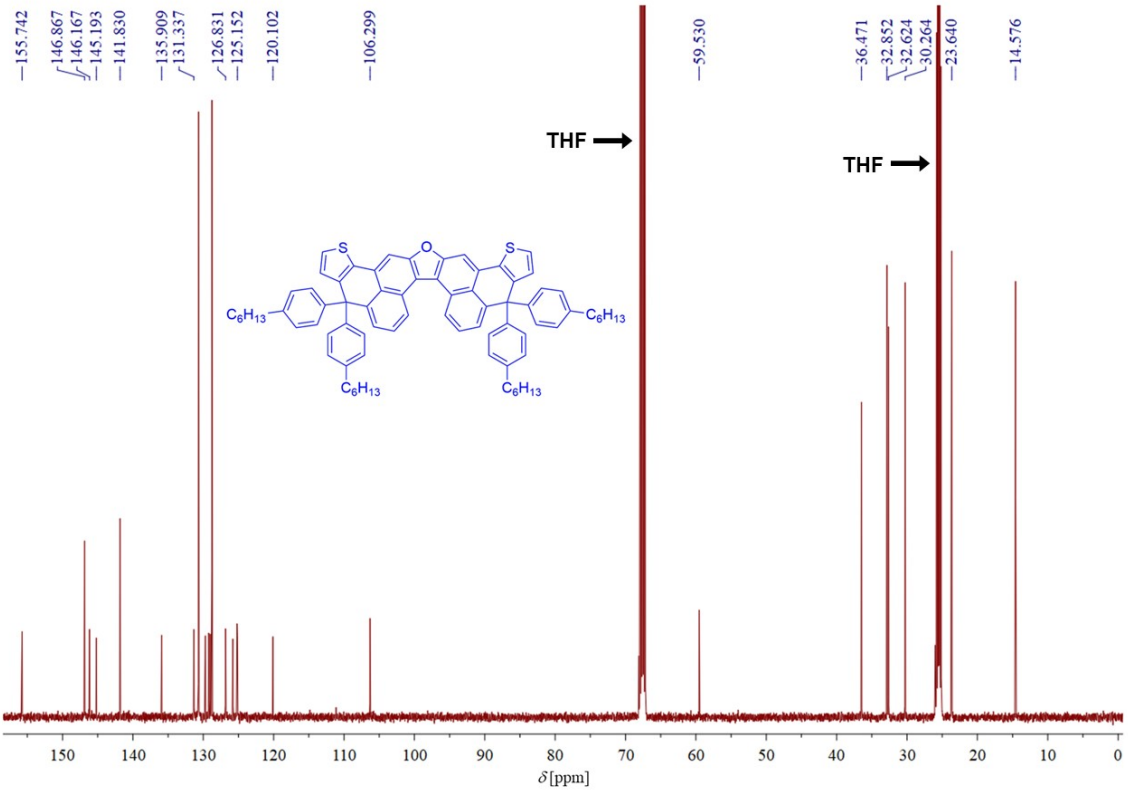

Fig. S33 [13]C NMR (125 MHz) spectrum of **DTPF4** in THF-d_8.

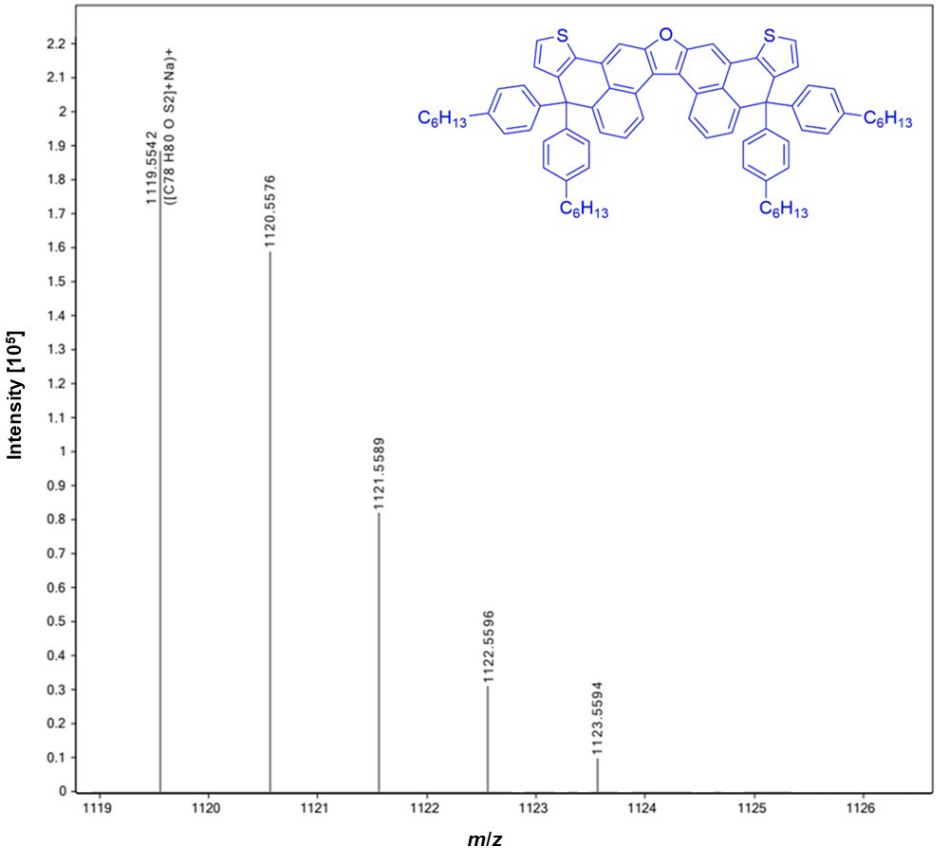

Fig. S34 High-resolution mass spectrum (ESI) of **DTPF4**.

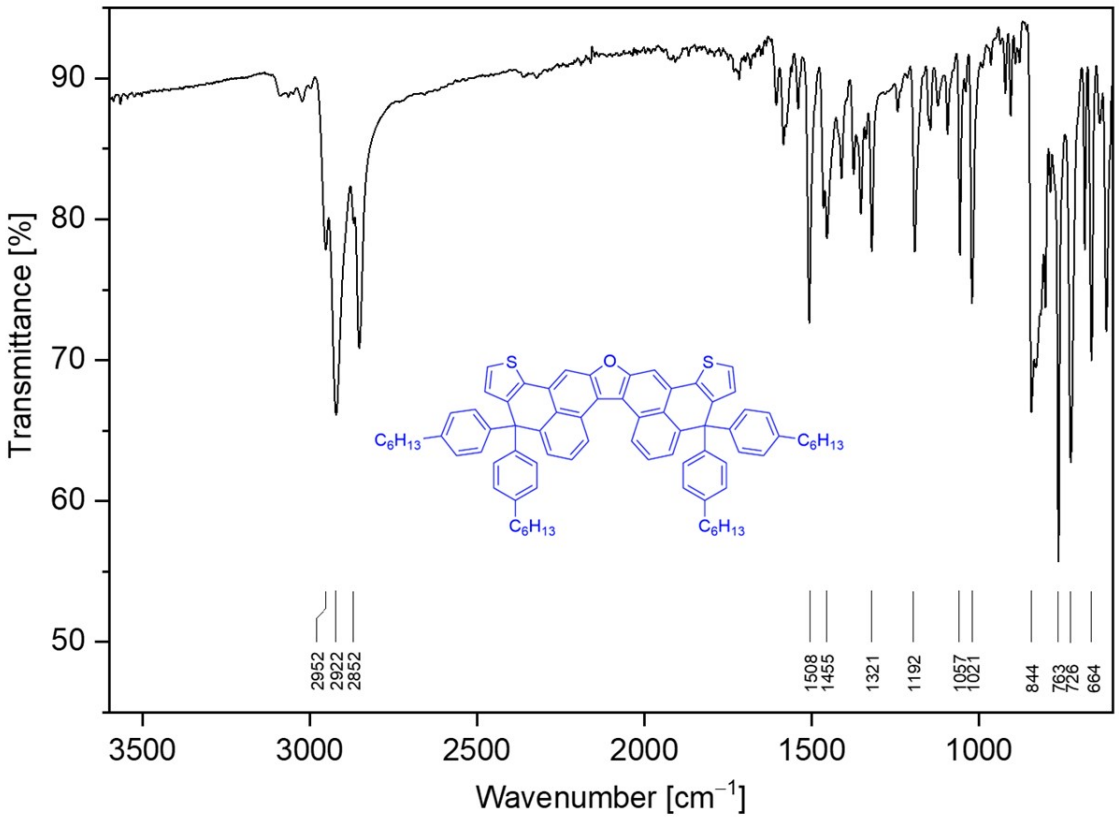

Fig. S35 ATR-FTIR spectrum of **DTPF4**.

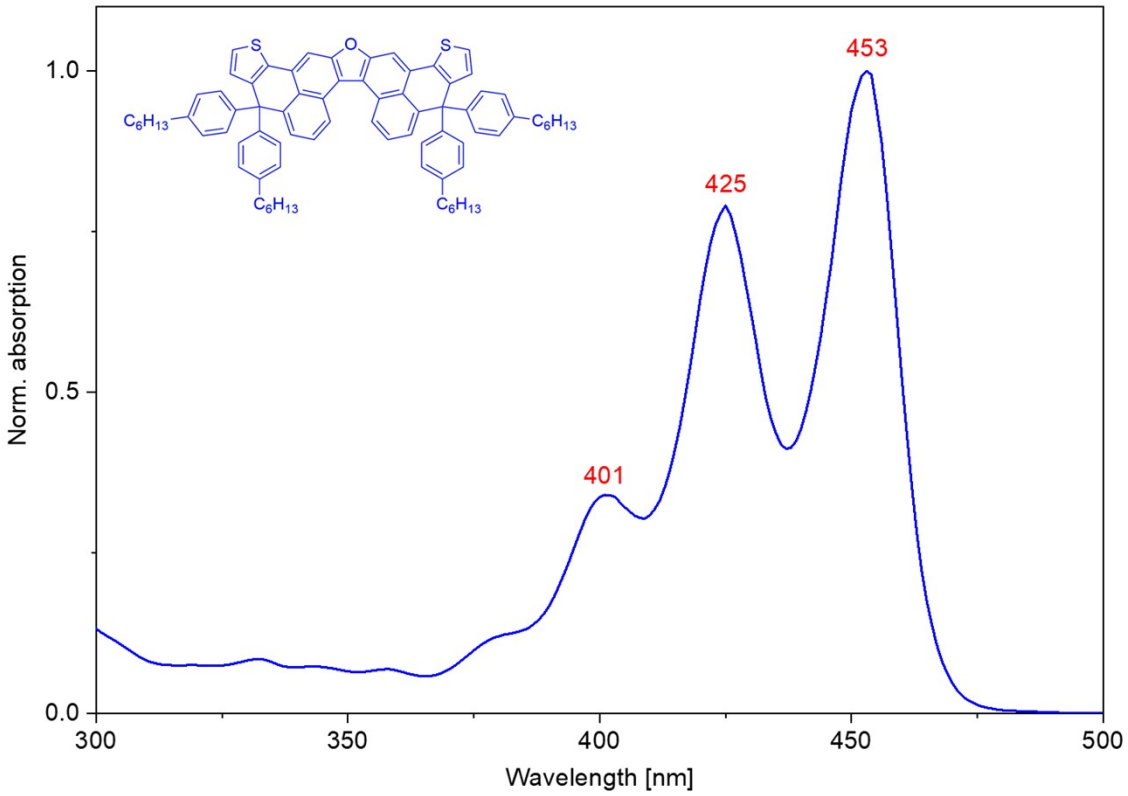

Fig. S36 UV-vis absorption spectrum of **DTPF4** in tetrahydrofuran.

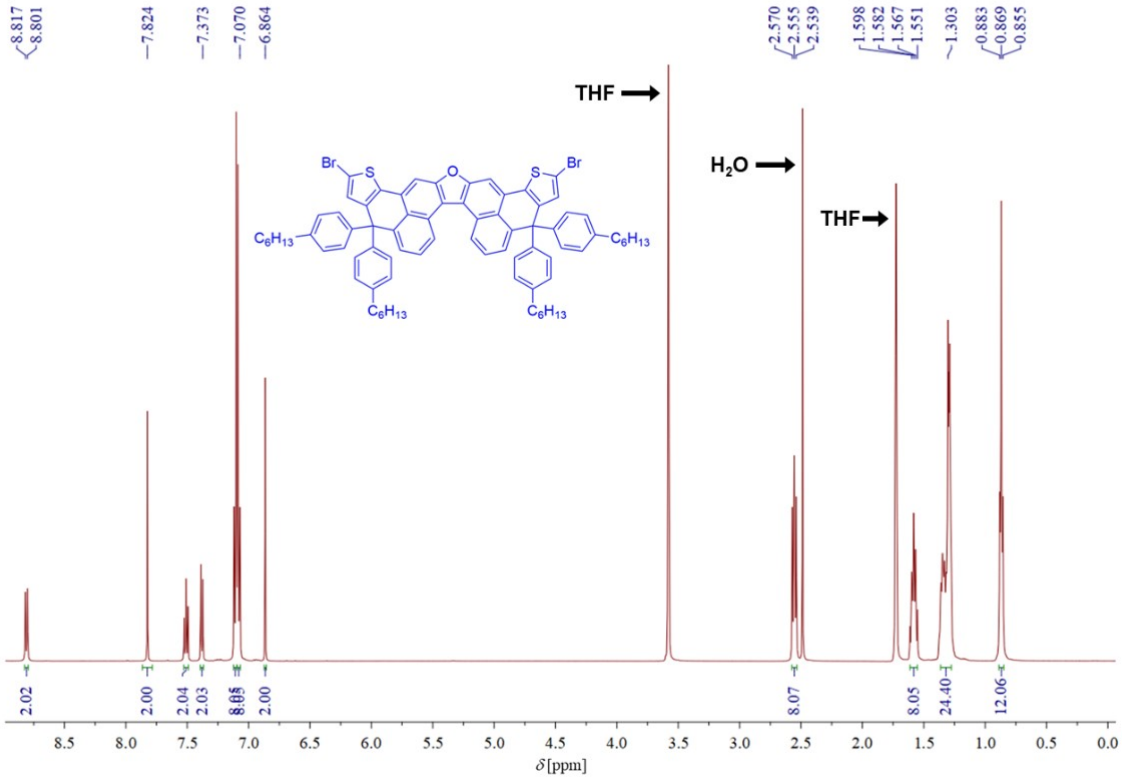

Fig. S37 ^{1}H NMR (500 MHz) spectrum of **DTPF4-2Br** in THF-d_8.

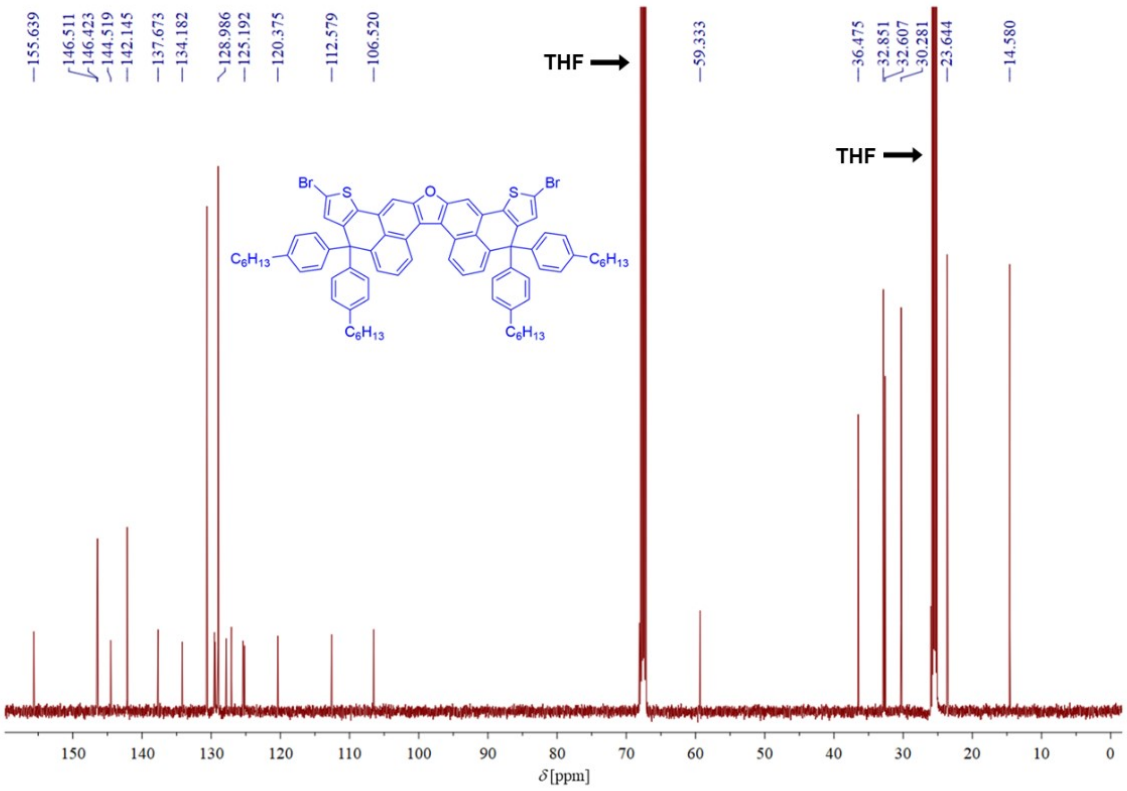

Fig. S38 ^{13}C NMR (125 MHz) spectrum of **DTPF4-2Br** in THF-d_8.

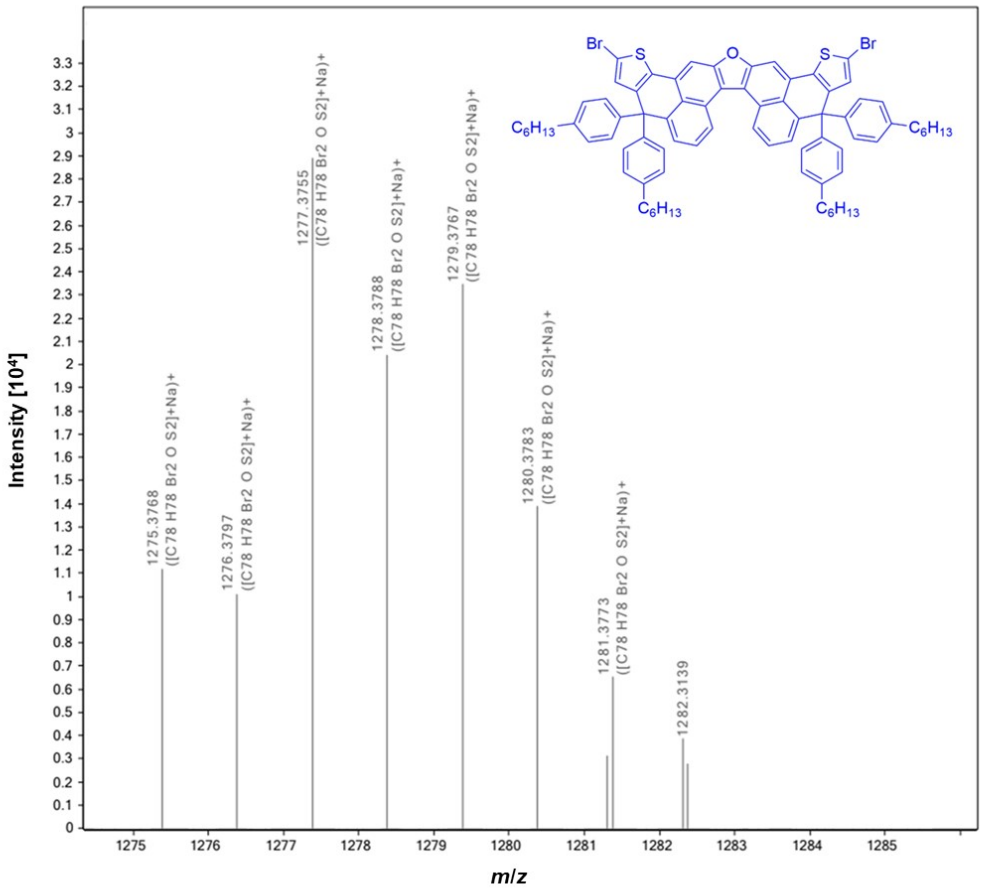

Fig. S39 High-resolution mass spectrum (ESI) of **DTPF4-2Br**.

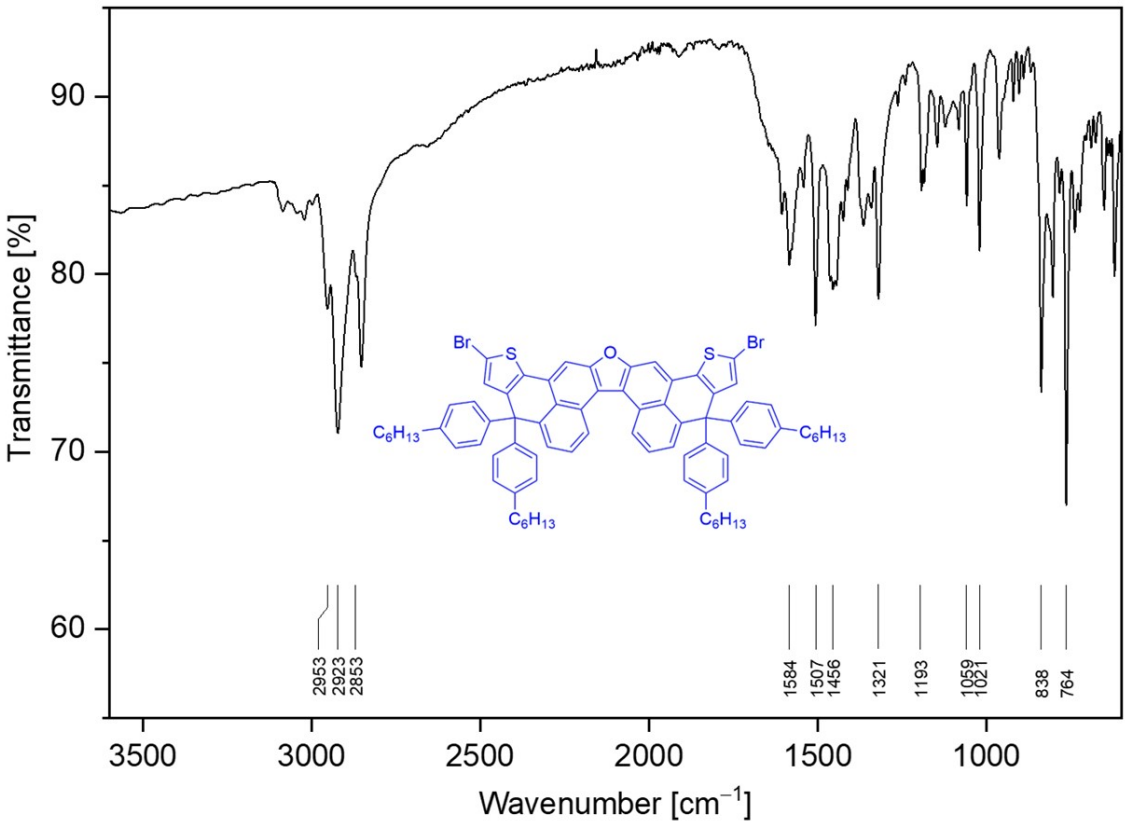

Fig. S40 ATR-FTIR spectrum of **DTPF4-2Br**.

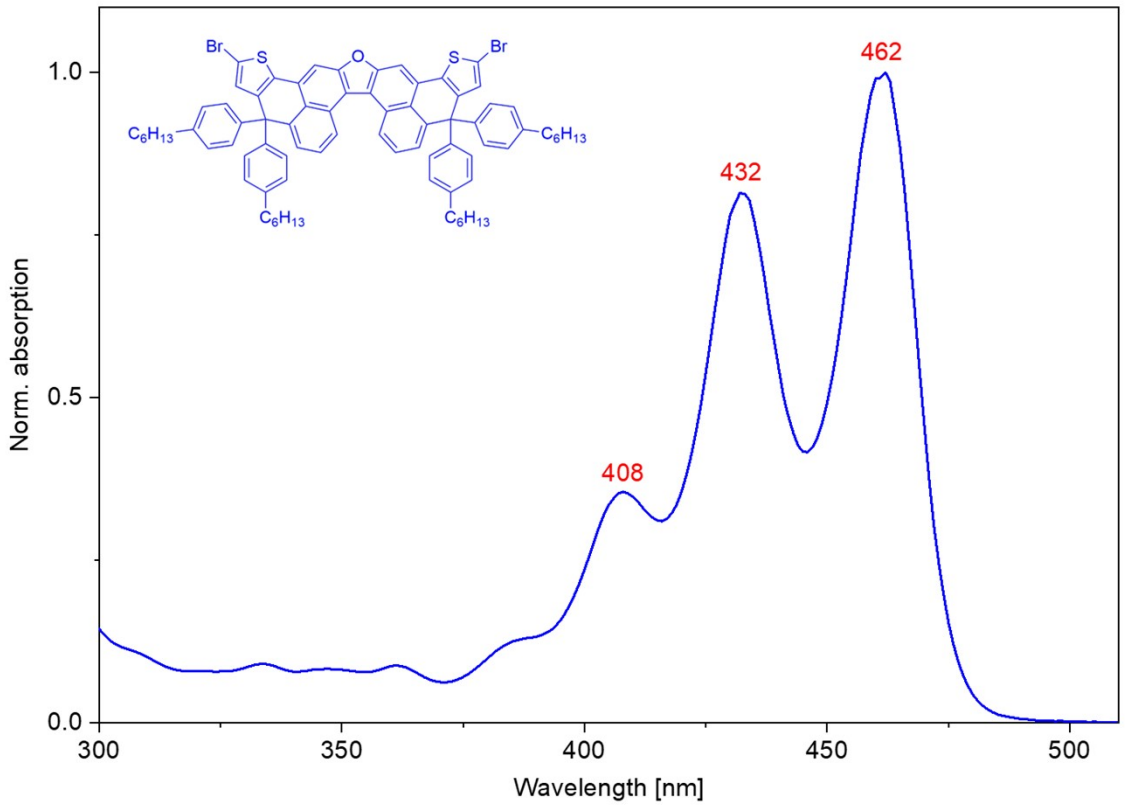

Fig. S41 UV-vis absorption spectrum of **DTPF4-2Br** in tetrahydrofuran.

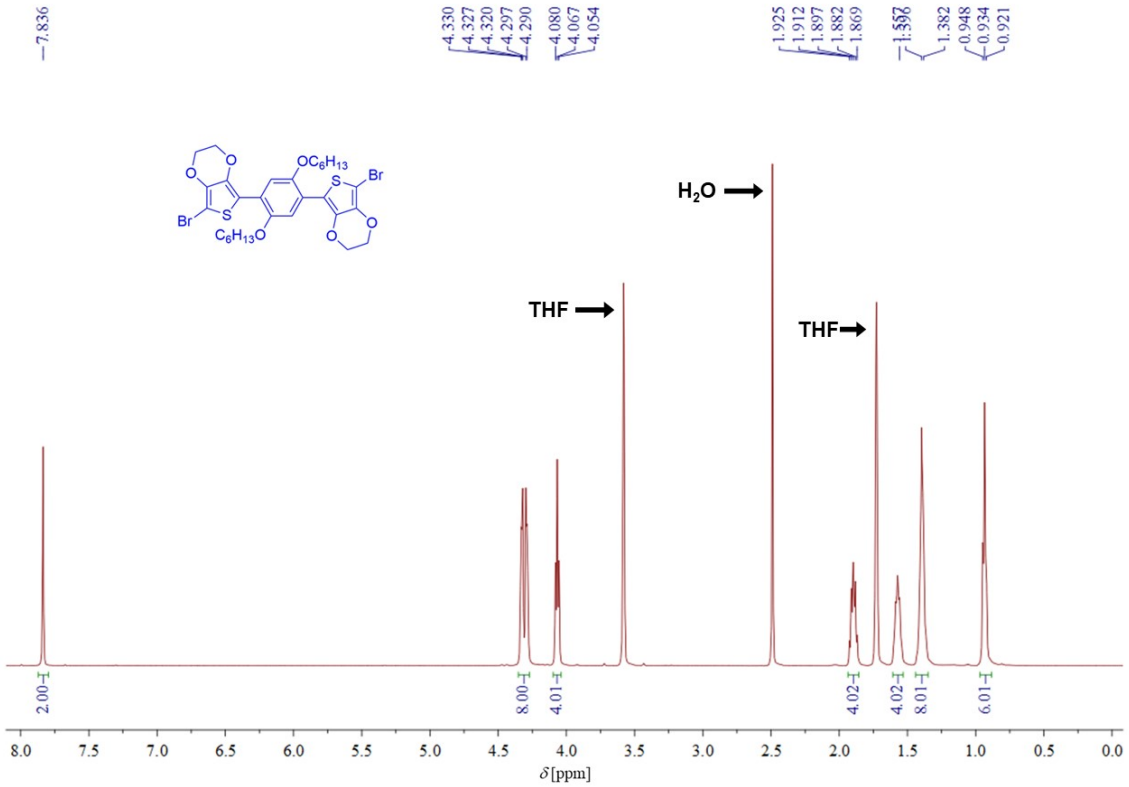

Fig. S42 [1]H NMR (500 MHz) spectrum of **EBEH-2Br** in THF-d_8.

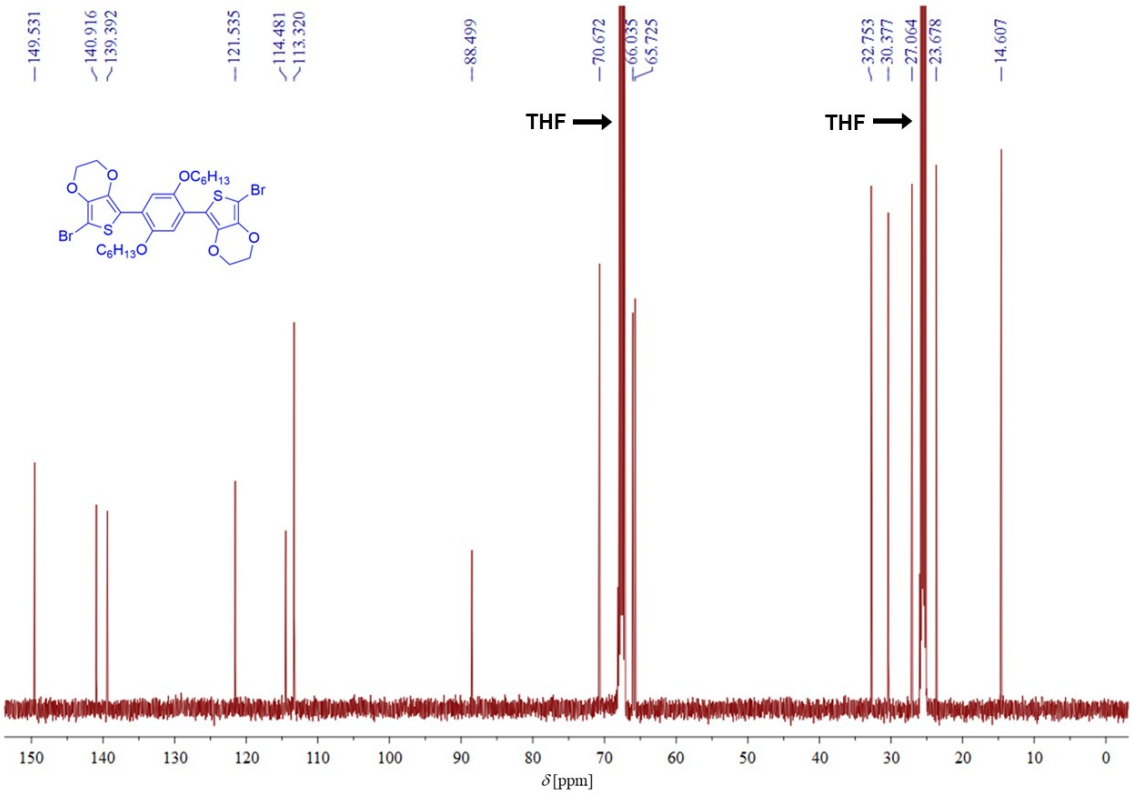

Fig. S43 [13]C NMR (125 MHz) spectrum of **EBEH-2Br** in THF-d_8.

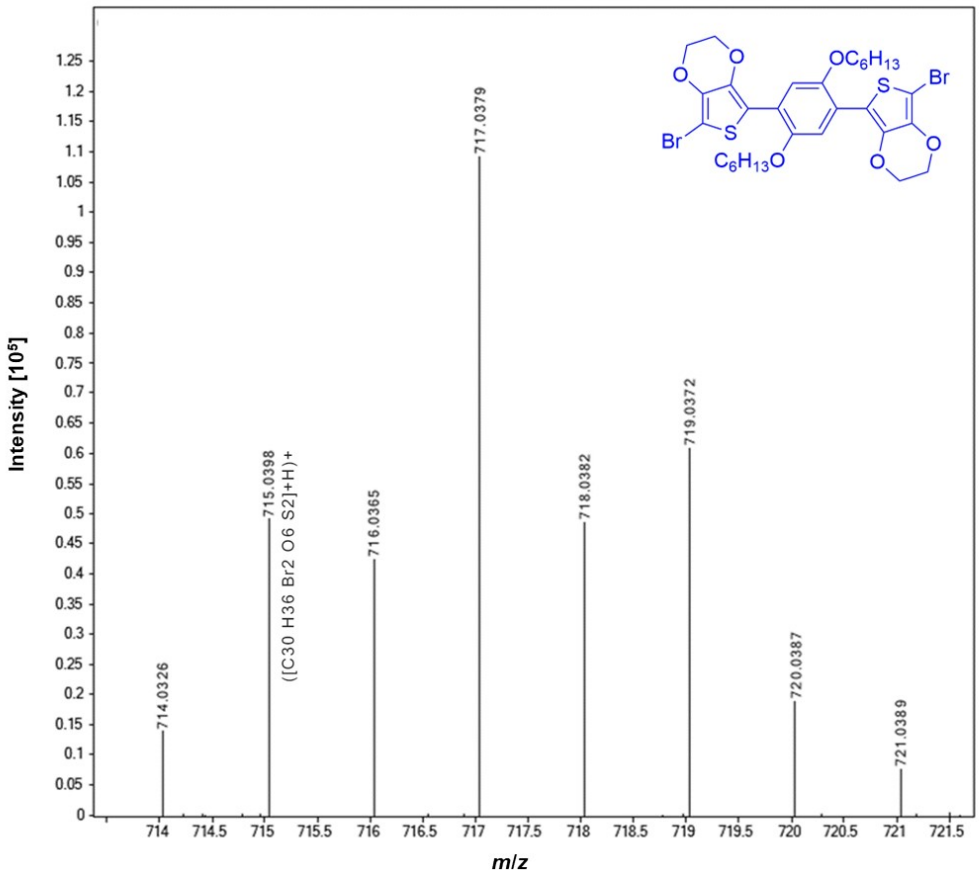

Fig. S44 High-resolution mass spectrum (ESI) of **EBEH-2Br**.

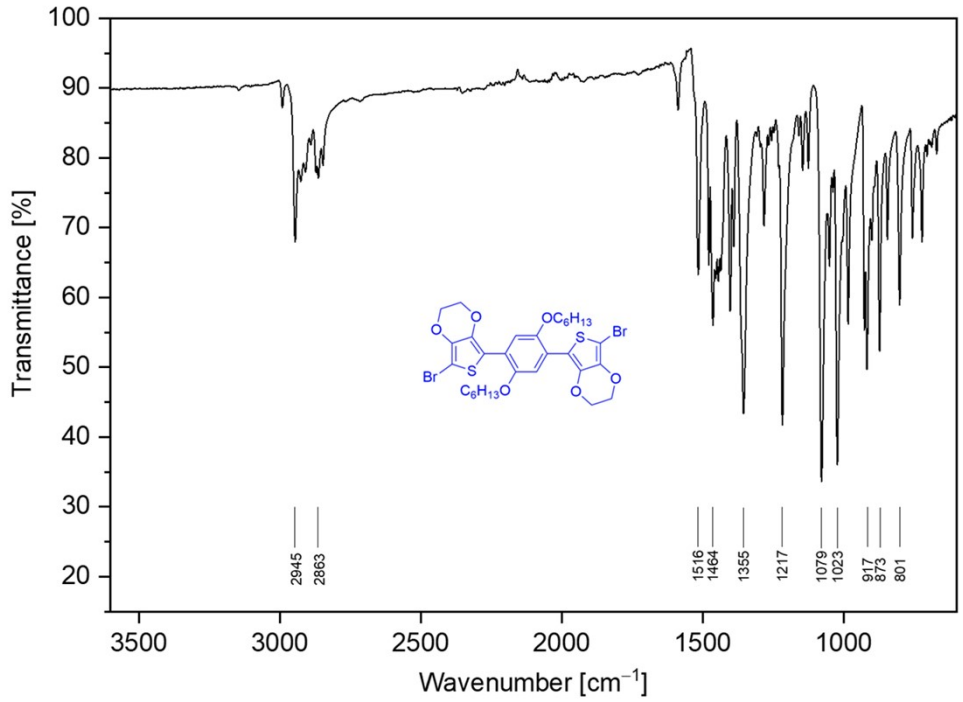

Fig. S45 ATR-FTIR spectrum of **EBEH-2Br**.

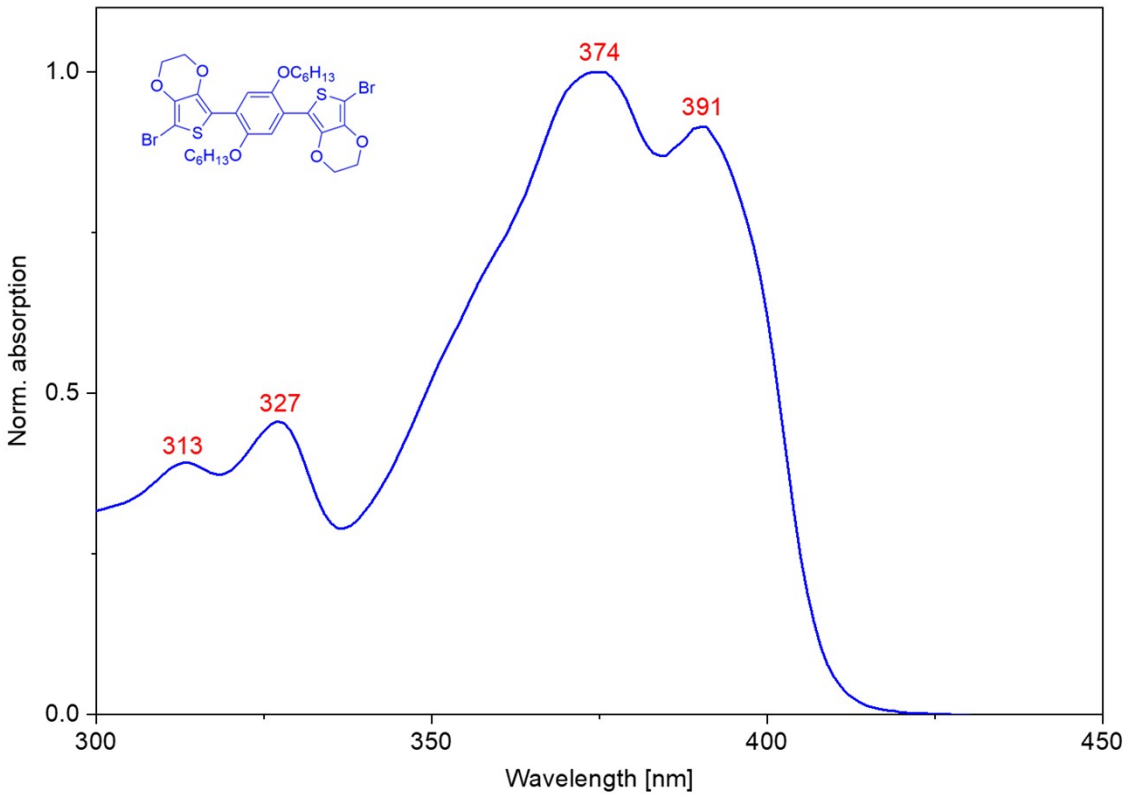

Fig. S46 UV-vis absorption spectrum of **EBEH-2Br** in tetrahydrofuran.

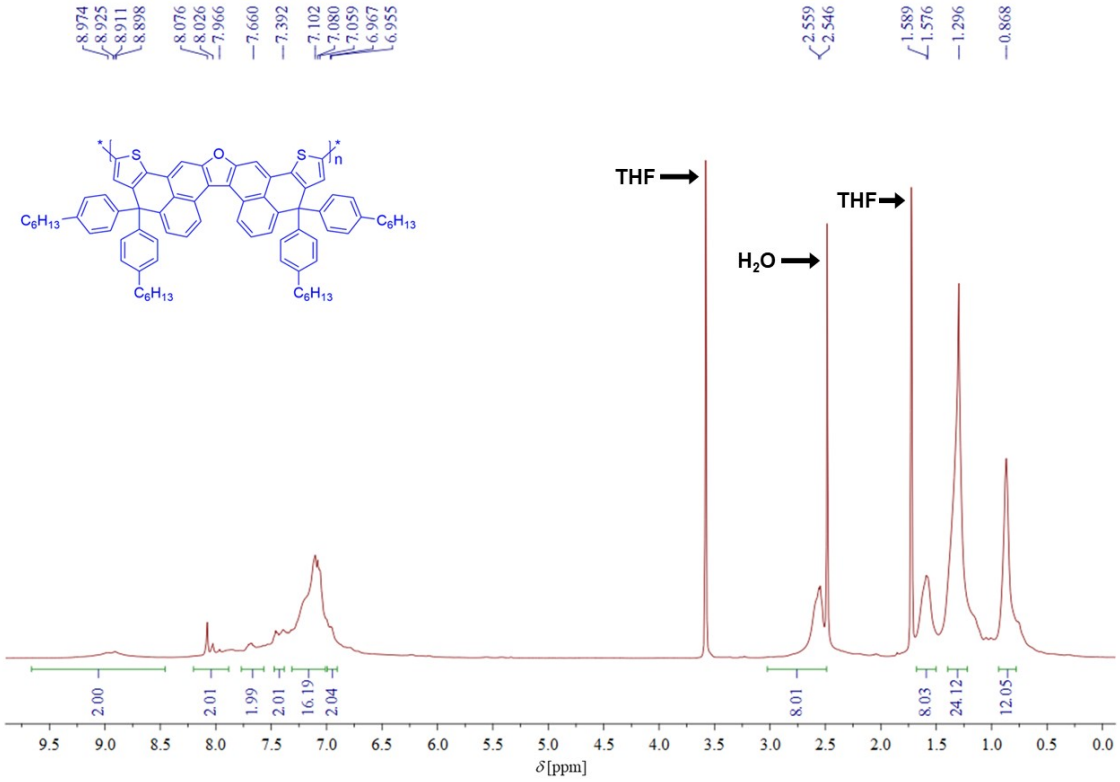

Fig. S47 ^{1}H NMR (500 MHz) spectrum of **p-DTPF4** in THF-d_8. Due to aggregation, it is hard to record a high-quality spectrum.

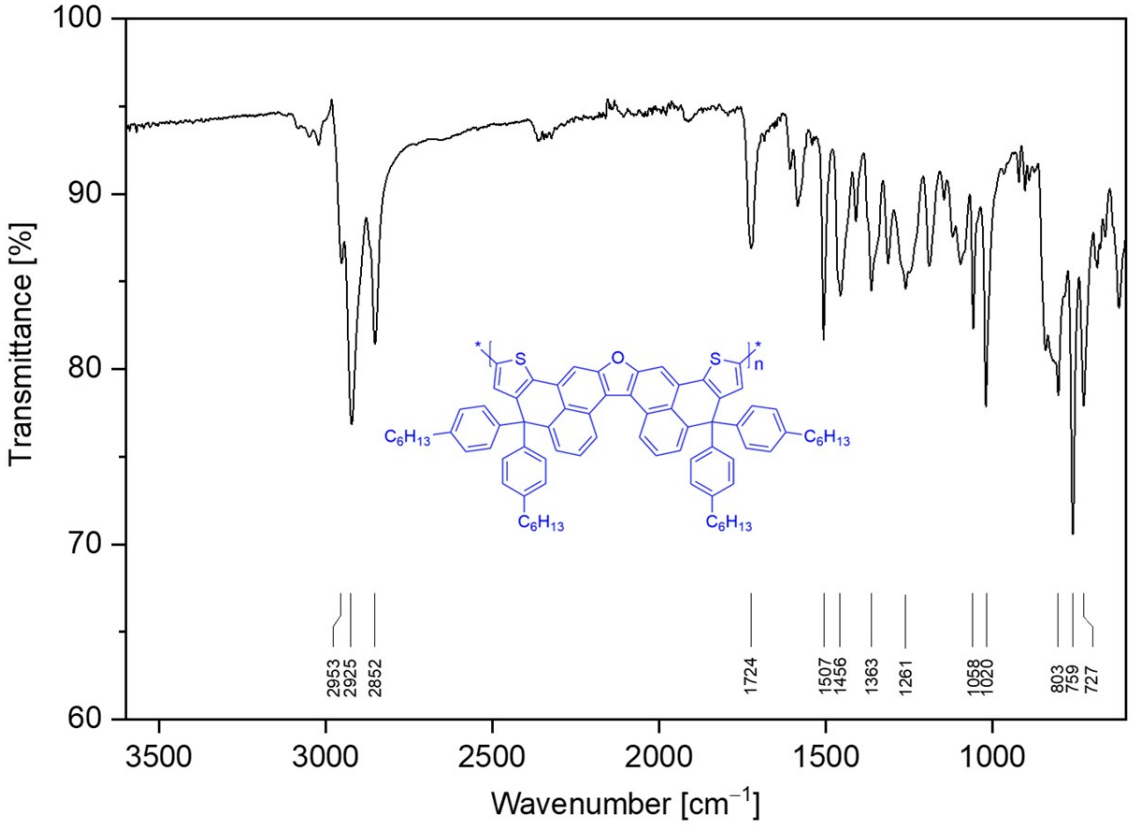

Fig. S48 ATR-FTIR spectrum of **p-DTPF4**.

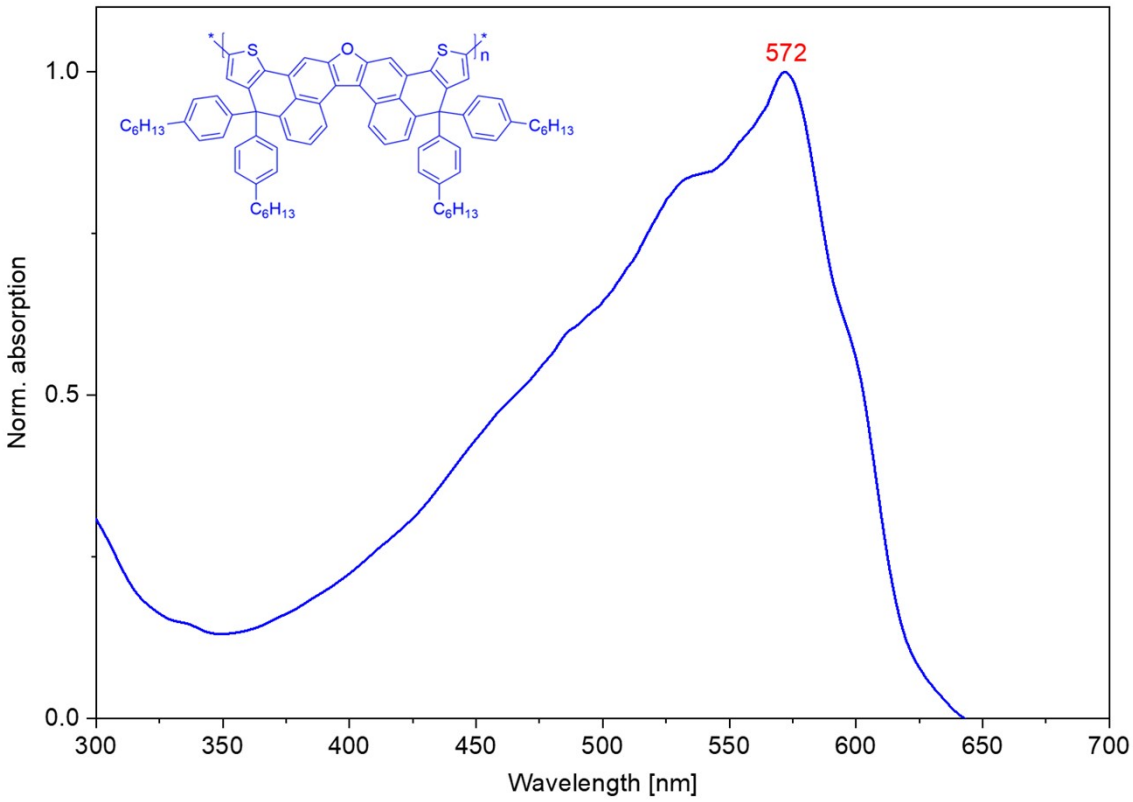

Fig. S49 UV-vis absorption spectrum of **p-DTPF4** in tetrahydrofuran.

Calibration Used: 2023/9/7 9:17:14

High Limit MW RT: 11.30 mins
High Limit MW: 5833811
K: 17.5000

Low Limit MW RT: 17.52 mins
Low Limit MW: 542
Alpha: 0.6700

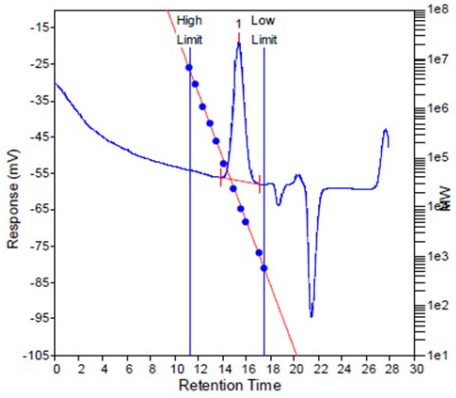

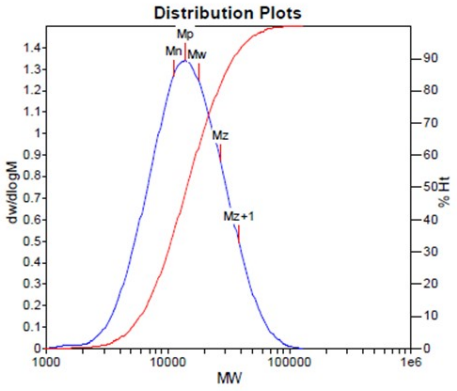

MW Averages

Peak No	Mp	Mn	Mw	Mz	Mz+1	Mv	PD
1	13794	11136	17685	26943	38374	16436	1.58809

Fig. S50 High-temperature gel permeation chromatography analysis of **p-DTPF4**.

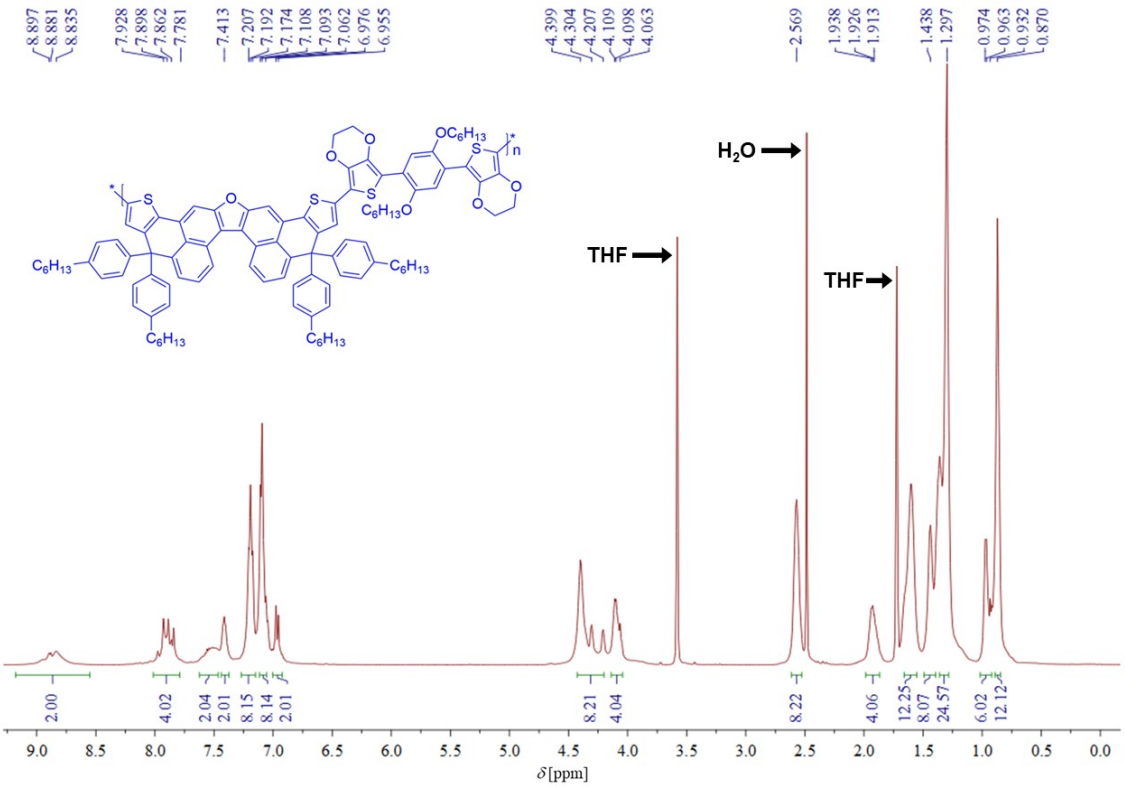

Fig. S51 ^{1}H NMR (500 MHz) spectrum of **p-DTPF4-EBEH** in THF-d_8. Due to aggregation, it is hard to record a high-quality spectrum.

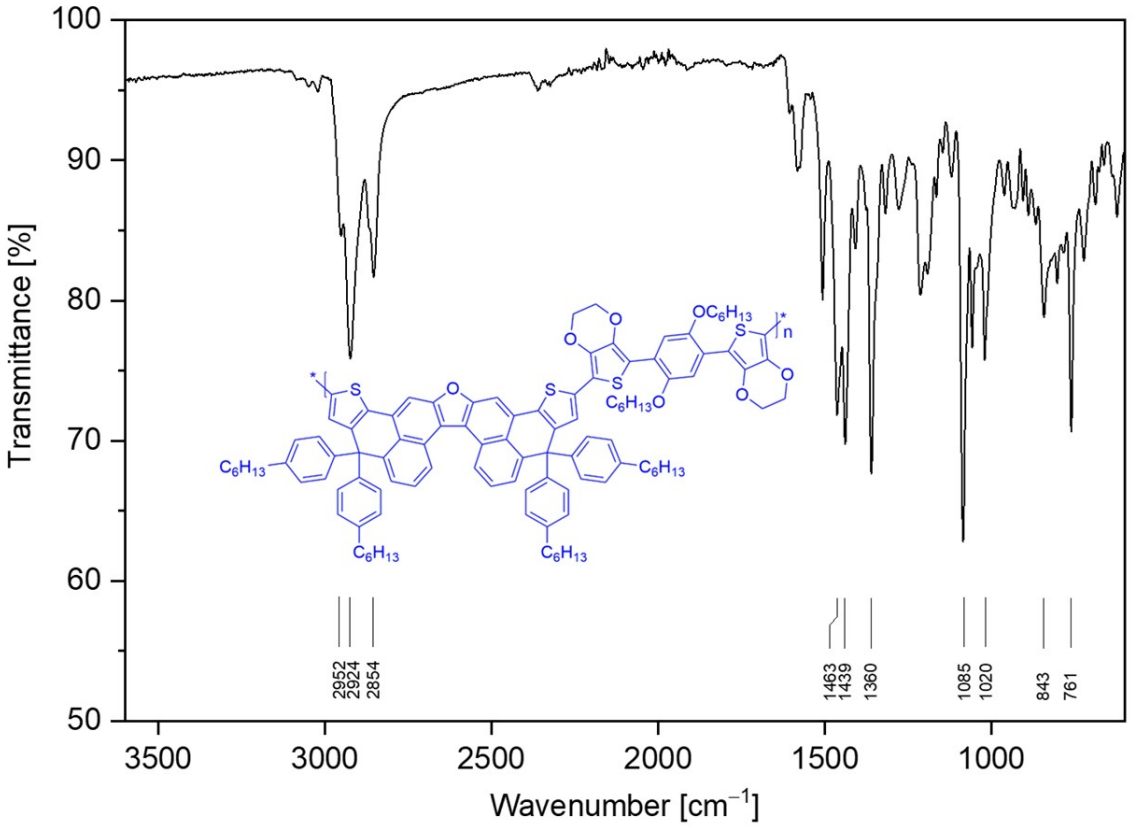

Fig. S52 ATR-FTIR spectrum of **p-DTPF4-EBEH**.

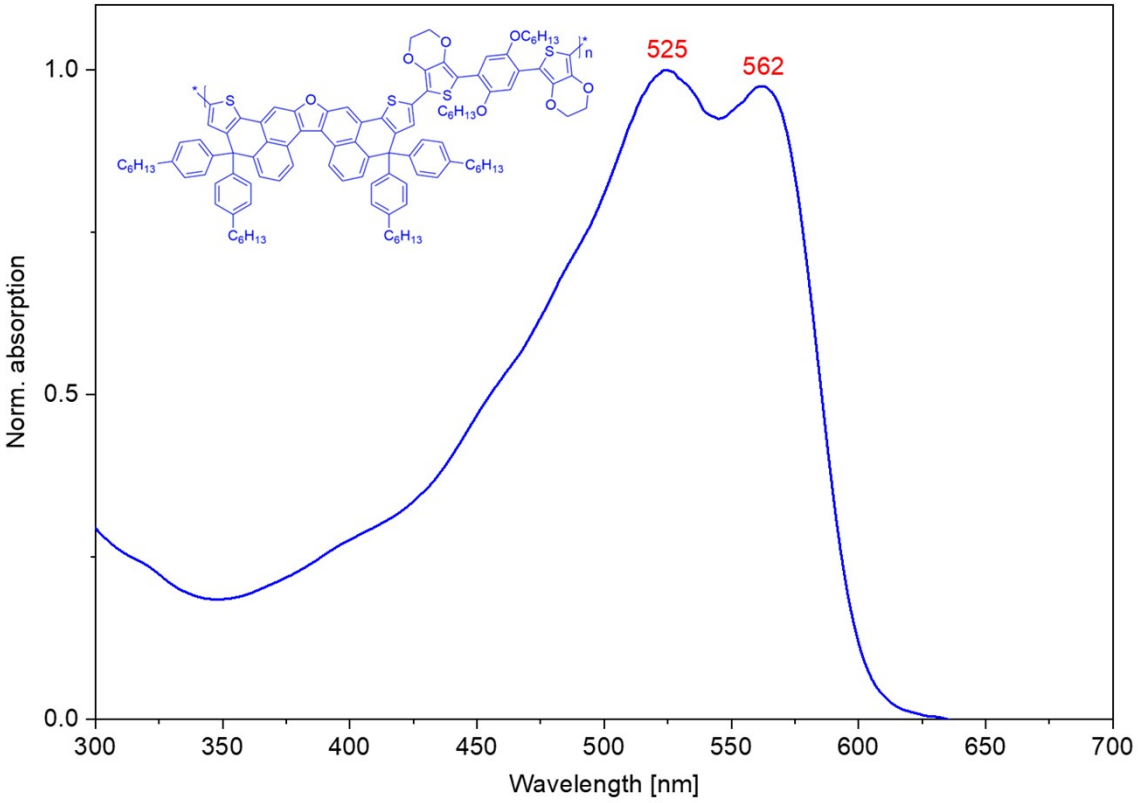

Fig. S53 UV-vis absorption spectrum of **p-DTPF4-EBEH** in tetrahydrofuran.

Calibration Used: 2023/2/17 17:23:31

High Limit MW RT: 10.88 mins
High Limit MW: 5636416
K: 17.5000

Low Limit MW RT: 17.10 mins
Low Limit MW: 636
Alpha: 0.6700

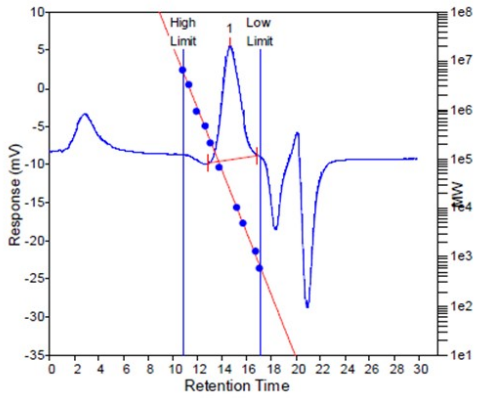

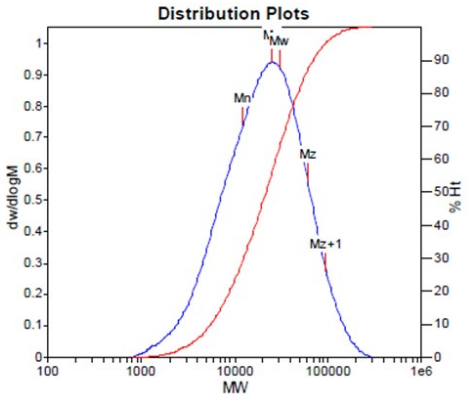

MW Averages

Peak No	Mp	Mn	Mw	Mz	Mz+1	Mv	PD
1	25223	12326	30856	60638	95693	27091	2.50333

Fig. S54 High-temperature gel permeation chromatography analysis of **p-DTPF4-EBEH**.

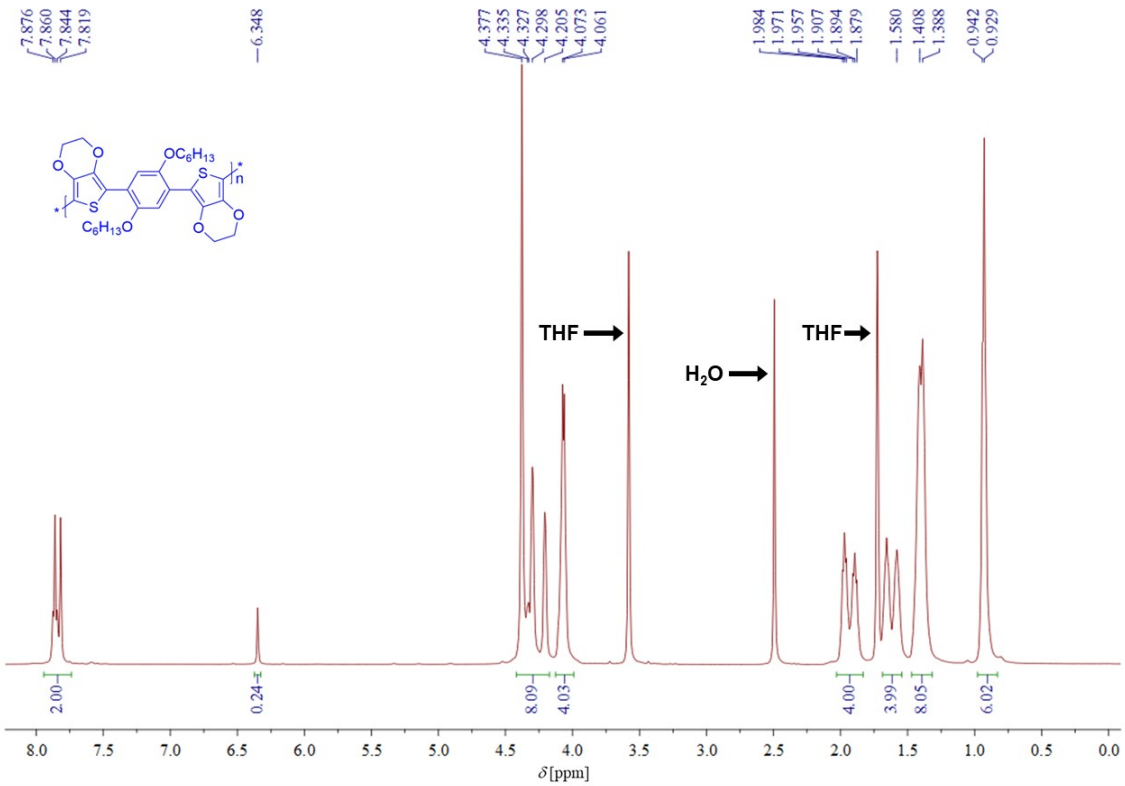

Fig. S55 ^{1}H NMR (500 MHz) spectrum of **p-EBEH** in THF-d_8.

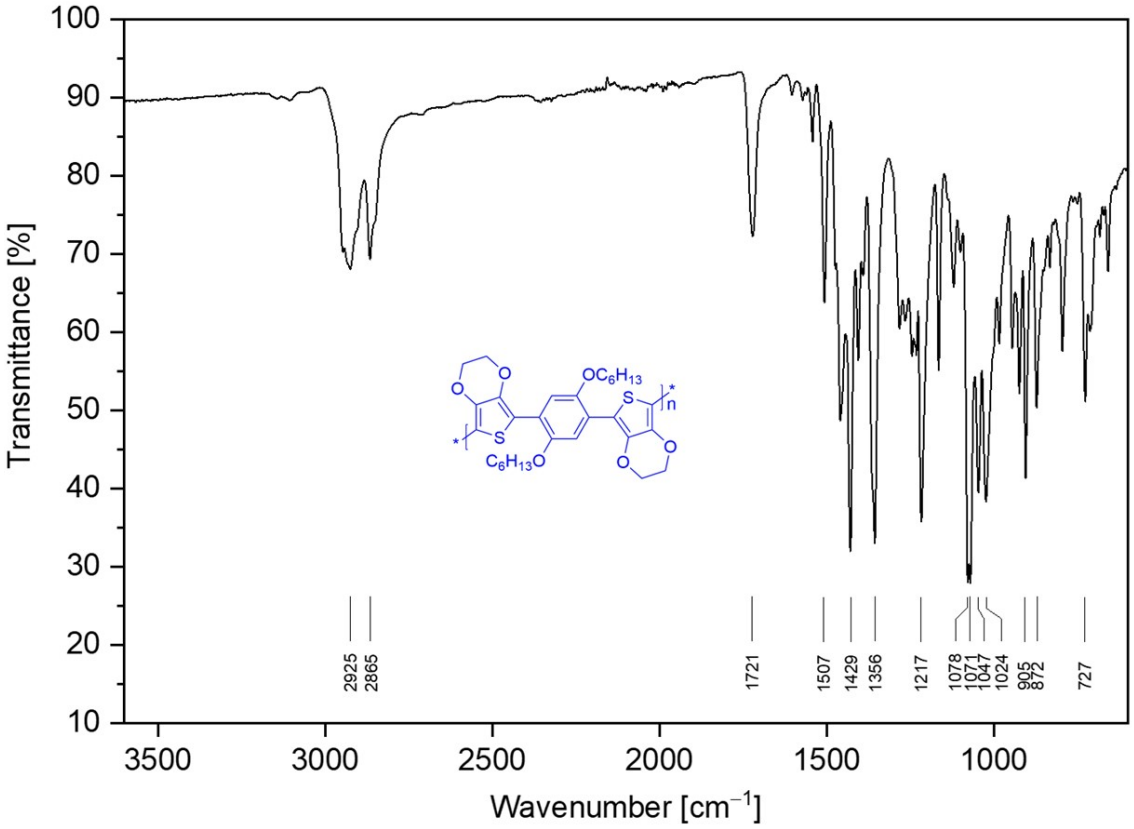

Fig. S56 ATR-FTIR spectrum of **p-EBEH**.

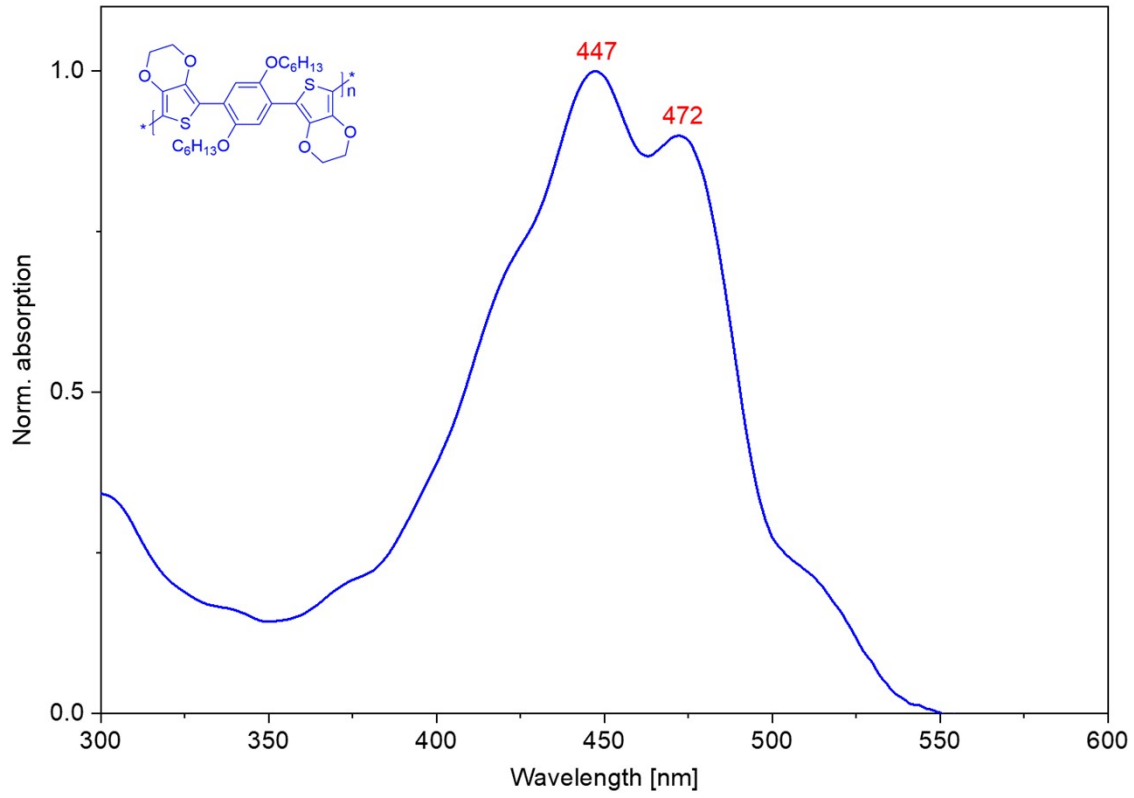

Fig. S57 UV-vis absorption spectrum of **p-EBEH** in tetrahydrofuran.

Calibration Used: 2023/9/7 9:17:14

High Limit MW RT: 11.30 mins

High Limit MW: 5833811

K: 17.5000

Low Limit MW RT: 17.52 mins

Low Limit MW: 542

Alpha: 0.6700

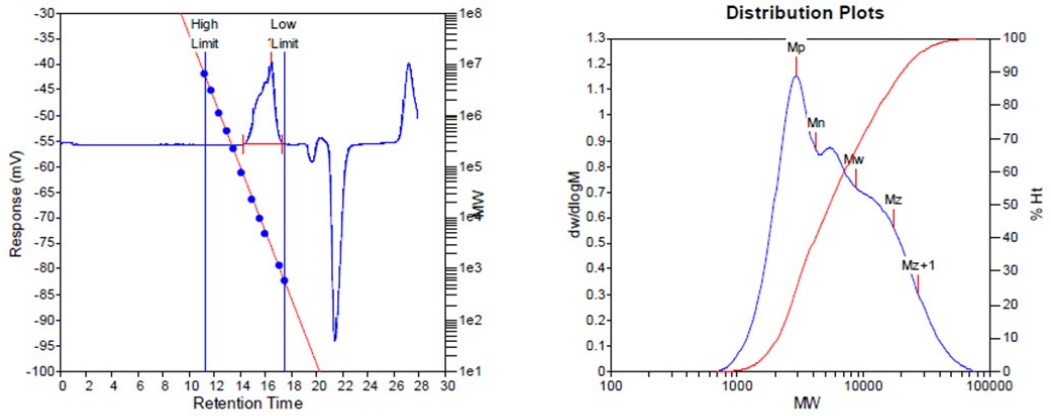

MW Averages

Peak No	Mp	Mn	Mw	Mz	Mz+1	Mv	PD
1	2948	4210	8674	17391	27144	7623	2.06033

Fig. S58 High-temperature gel permeation chromatography analysis of **p-EBEH**.

5 References

1 V. Akhmetov, M. Feofanov, C. Ruppenstein, J. Lange, D. Sharapa, M. Krstić, F. Hampel, E. A. Kataev and K. Amsharov, *Chem. Eur. J.*, 2022, **28**, e202200584.

2 N. Cai, R. Li, Y. Wang, M. Zhang and P. Wang, *Energy Environ. Sci*., 2013, **6**, 139.

3 S. Ming, K. Lin, H. Zhang, F. Jiang, P. Liu, J. Xu, G. Nie and X. Duan, *Chem*. *Commun.*, 2020, **56**, 5275.

4 Y. Ren, M. Ren, X. Xie, J. Wang, Y. Cai, Y. Yuan, J. Zhang and P. Wang, *Nano Energy*, 2021, **81**, 105655.

5 W. C. Oliver and G. M. Pharr, *J. Mater. Res.*, 1992, **7**, 1564.

6 Y. Zhao, F. Ma, Z. Qu, S. Yu, T. Shen, H.-X. Deng, X. Chu, X. Peng, Y. Yuan, X. Zhang and J. You, *Science*, 2022, **377**, 531.

7 T. Li, Y. Zhang, M. Ren, Y. Mu, J. Zhang, Y. Yuan, M. Zhang and P. Wang, *Angew. Chem. Int. Ed.*, 2024, **63**, e202401604.

8 Q. Jiang, Y. Zhao, X. Zhang, X. Yang, Y. Chen, Z. Chu, Q. Ye, X. Li, Z. Yin and J. You, *Nat. Photon.*, 2019, **13**, 460.

9 C. M. Cardona, W. Li, A. E. Kaifer, D. Stockdale and G. C. Bazan, *Adv. Mater.*, 2011, **23**, 2367.